Small-Scale Properties of Turbulent Rayleigh-Bénard Convection

Detlef Lohse[1] and Ke-Qing Xia[2]

[1]Physics of Fluids Group, Department of Science and Technology, J.M. Burgers Center for Fluid Dynamics, and Impact-Institute, University of Twente, 7500 AE Enschede, The Netherlands; email: d.lohse@utwente.nl

[2]Department of Physics, The Chinese University of Hong Kong, Shatin, Hong Kong, China; email: kxia@phy.cuhk.edu.hk

Annu. Rev. Fluid Mech. 2010. 42:335–64

First published online as a Review in Advance on September 2, 2009

The *Annual Review of Fluid Mechanics* is online at fluid.annualreviews.org

This article's doi: 10.1146/annurev.fluid.010908.165152

0066-4189/10/0115-0335$20.00

Key Words

thermal convection, turbulence, structure functions, Bolgiano scaling

Abstract

The properties of the structure functions and other small-scale quantities in turbulent Rayleigh-Bénard convection are reviewed, from an experimental, theoretical, and numerical point of view. In particular, we address the question of whether, and if so where in the flow, the so-called Bolgiano-Obukhov scaling exists, i.e., $S_\theta(r) \sim r^{2/5}$ for the second-order temperature structure function and $S_u(r) \sim r^{6/5}$ for the second-order velocity structure function. Apart from the anisotropy and inhomogeneity of the flow, insufficiently high Rayleigh numbers, and intermittency corrections (which all hinder the identification of such a potential regime), there are also reasons, as a matter of principle, why such a scaling regime may be limited to at most a decade, namely the lack of clear scale separation between the Bolgiano length scale L_B and the height of the cell.

1. INTRODUCTION

Thermally driven turbulence is of tremendous importance to various areas of science, technology, and the environment and in the geophysical and astrophysical context. For flow in the atmosphere, thermal convection (e.g., see Hartmann et al. 2001) is relevant both on smaller length scales and timescales for weather predictions and on larger scales for climate calculations. In the ocean (e.g., see Marshall & Schott 1999), thermohaline convection (Rahmstorf 2000) is a main driving mechanism of deep-ocean circulation. Thermally driven convection takes place both in Earth's outer core (see, e.g., Cardin & Olson 1994) and in its mantle (see, e.g., McKenzie et al. 1974).

The idealized system of thermally driven turbulence is turbulent Rayleigh-Bénard (RB) convection—a fluid in a box of height L strongly heated from below and cooled from above. This system may even be considered as a raw model for turbulent flow in general. It is not only a mathematically well-defined problem, in principle given by the Boussinesq equations (see Section 2) and the appropriate boundary conditions for the velocity field $\boldsymbol{u}(\boldsymbol{x}, t)$ and the temperature field $\theta(\boldsymbol{x}, t)$, but it can also be straightforwardly realized experimentally. **Figure 1** shows a shadowgraph image of turbulent thermal convection in an aspect-ratio-one cylindrical cell, together with two instantaneous two-dimensional (2D) velocity field snapshots, taken with particle image velocimetry (PIV).

In contrast, the theoretical concept of homogeneous and isotropic turbulence (e.g., see Batchelor 1953, Frisch 1995, Kolmogorov 1941, Monin & Yaglom 1975, Pope 2000) is much harder to realize in a laboratory. Nonetheless, most theoretical (Frisch 1995; e.g., for a more recent review, see Falkovich et al. 2001) and numerical (recently reviewed in Ishihara et al. 2009) work on the (small scale) scaling of structure functions (SFs) and energy spectra focused on

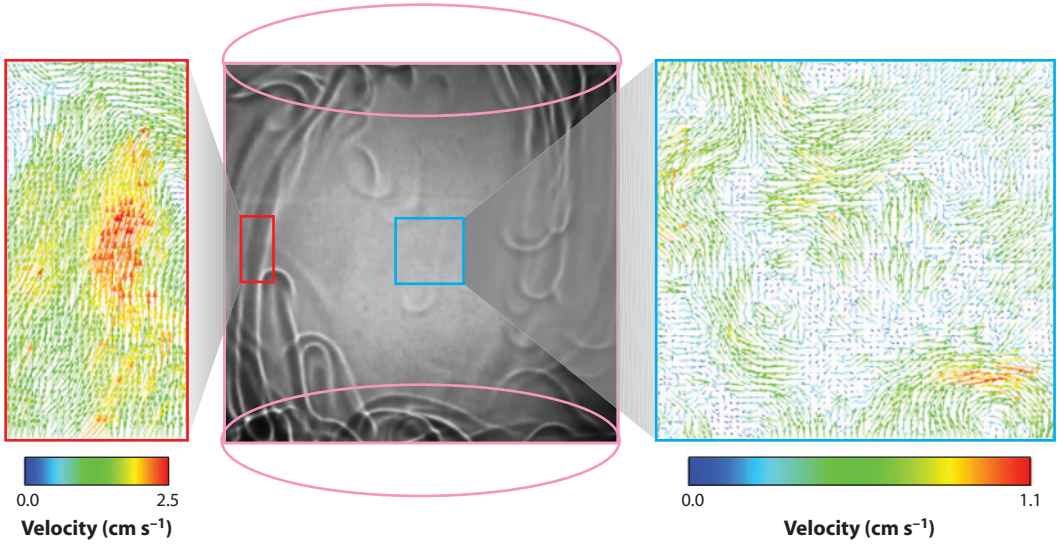

Figure 1

(*Middle panel*) Shadowgraph image of turbulent thermal convection in an aspect-ratio-one cylindrical cell (Ra = 6.8×10^8, Pr = 596). The thermal plumes in the image play important roles in the small-scale properties of the system's velocity and temperature fields. (*Left and right panels*) Instantaneous high-resolution 2D velocity field measured in the sidewall (*left panel*) and central regions (*right panel*) marked by the red rectangle and blue square in the shadowgraph, respectively. Because of the large disparity in the number of plumes, these two regions exhibit different scaling properties of velocity and temperature fields, as found by Sun et al. (2006). Shadowgraph taken from Xi et al. 2004, PIV taken from Zhou et al. 2008.

homogeneous, isotropic turbulence, comparing these results with laboratory and field measurements for which the conditions of homogeneity and isotropy were only approximately fulfilled. In their *Annual Review of Fluid Mechanics* article, Sreenivasan & Antonia (1997) describe the phenomenology of this small-scale turbulence. In the inertial range, the second-order velocity SF $S_u(r) = \langle(\boldsymbol{u}(\boldsymbol{x}+\boldsymbol{r}) - \boldsymbol{u}(\boldsymbol{x}))^2\rangle_{\boldsymbol{x},t}$ is basically found to scale with the Kolmogorov (1941) scaling $\sim r^{2/3}$, in short called K41, apart from small intermittency corrections, which are found to be remarkably universal (Arneodo et al. 1996). K41 follows from pure dimensional analysis, assuming that in the inertial range, apart from the scale r itself, the only relevant parameter is the mean energy dissipation rate ϵ_u, giving

$$S_u(r) \sim (\epsilon_u r)^{2/3}. \tag{1}$$

Obukhov (1949) and Corrsin (1951) generalized Kolmogorov's argument to the fluctuations of a passive scalar $\theta(\boldsymbol{x}, t)$, giving

$$S_\theta(r) \sim \epsilon_\theta \epsilon_u^{-1/3} r^{2/3} \tag{2}$$

for the second-order SF $S_\theta(r) = \langle(\theta(\boldsymbol{x}+\boldsymbol{r}) - \theta(\boldsymbol{x}))^2\rangle_{\boldsymbol{x},t}$ of $\theta(\boldsymbol{x}, t)$. Here ϵ_θ is its dissipation rate. Again, apart from small intermittency corrections, Equation 2 is in reasonable agreement with the experimental data (see Warhaft 2000).

In analogy to K41, pure dimensional analysis can also be done for RB turbulence. Assuming that next to the scale r, the only relevant parameters are the mean thermal dissipation rate ϵ_θ and the product of the thermal expansion coefficient β and gravity g, one obtains the so-called Bolgiano-Obukhov scaling (BO59), which was first suggested for stably stratified convection (Bolgiano 1959, Obukhov 1959). It reads

$$S_u(r) \sim \epsilon_\theta^{2/5} (\beta g)^{4/5} r^{6/5}, \tag{3}$$

$$S_\theta(r) \sim \epsilon_\theta^{4/5} (\beta g)^{-2/5} r^{2/5}. \tag{4}$$

According to the same dimensional argument, the mixed SF between temperature and vertical velocity $S_{\theta u_3}(r) = \langle(\theta(\boldsymbol{x}+\boldsymbol{r}) - \theta(\boldsymbol{x}))(u_3(\boldsymbol{x}+\boldsymbol{r}) - u_3(\boldsymbol{x})\rangle_{\boldsymbol{x},t}$ should scale as

$$S_{\theta u_3}(r) \sim \epsilon_\theta^{3/5} (\beta g)^{1/5} r^{4/5}. \tag{5}$$

When comparing Equations 1 and 3, on one hand, or Equations 2 and 4, on the other hand, one can read off the so-called Bolgiano length L_B as crossover scale, with

$$L_B = \epsilon_u^{5/4} \epsilon_\theta^{-3/4} (\beta g)^{-3/2}. \tag{6}$$

For $L_B \ll r \ll L$, one expects BO59 scaling, whereas for $\eta \ll r \ll L_B$ one still expects K41 scaling (see **Figure 2**). (Here, the height L of the cell is identified with the outer length scale and $\eta = \nu^{3/4}/\epsilon^{1/4}$ is the Kolmogorov length, i.e., the inner length scale.) However, the scaling as sketched in **Figure 2** has hitherto not been identified in experimental or in numerical data, neither for the SFs nor in the respective Fourier transforms, for which BO59 would mean $E_u(k) \sim k^{-11/5}$ for the energy spectrum and $E_\theta(k) \sim k^{-7/5}$ for the thermal spectrum.

In this article we review the experimental and numerical attempts to at least partly identify BO59 scaling. Owing to space limitations, we do not strive to review all aspects of the problem that may be called small-scale. For example, we do not discuss the extraction and characterization of individual thermal plumes (Ching et al. 2004b, Funfschilling et al. 2008, Julien et al. 1999, Puthenveettil & Arakeri 2005, Shishkina & Wagner 2008, Zhou & Xia 2002, Zhou et al. 2007) and studies of the energy and thermal dissipation rates (Benzi et al. 1998, Ching & Kwok 2000, He & Tong 2009, He et al. 2007, Kaczorowski & Wagner 2009, Kerr 2001, Shishkina & Wagner 2006, Verzicco & Camussi 2003), nor do we review the small-scale properties in 2D turbulent

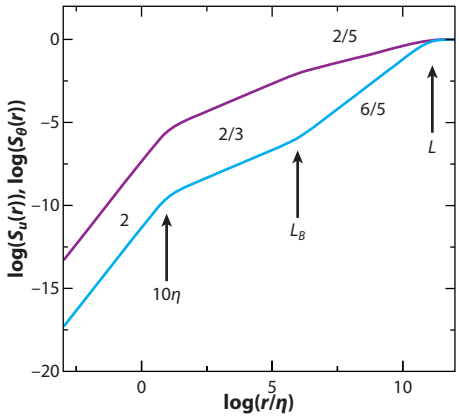

Figure 2

Sketch of the second-order velocity (*blue curve*) and temperature (*purple curve*) structure functions, as they follow from BO59 dimensional analysis: $L_B = 10^6\eta$ and $L = 10^{11}\eta$ are assumed, and there is a crossover at 10η (e.g., see Effinger & Grossmann 1987) between the viscous subrange and the inertial subrange. For $10\eta < r < L_B$, the BO59-type dimensional analysis gives K41 scaling (Equations 1 and 2), and for $L_B < r < L$ it gives BO59 scaling (Equations 3 and 4). Such pronounced scaling as sketched here has hitherto never been observed.

thermal convection (Celani et al. 2001, 2002; Zhang & Wu 2005; Zhang et al. 2005) and those in the Lagrangian frame (Gasteuil et al. 2007, Schumacher 2008). Rather, we focus on the issue regarding the existence of BO59 and how the properties of an active scalar as a small-scale quantity compare with those of a passive scalar in convective flows. Section 2 presents numerical data on the Bolgiano scale L_B (which turns out to be the crucial quantity) and demonstrates that the BO59 dimensional argument is too simplistic. We then point out further difficulties, both practical and as a matter of principle, in identifying BO59 scaling: the inhomogeneity and anisotropy of the flow and intermittency. Section 3 presents experimental and numerical data on the SFs, whereas Section 4 compares the flow characteristics of an active scalar, such as temperature in RB convection, with that of a passive scalar.

The review aims to give an update on the statistics of small-scale quantities in RB convection to the status as described in Siggia (1994). An update on large-scale quantities and in particular on how the Nusselt number (Nu) and the Reynolds number (Re) depend on the Rayleigh number (Ra) and the Prandtl number (Pr) has already been given by Ahlers et al. (2009). Along with Ra, Pr, and the shape of the cell, the other control parameter of the system is the aspect ratio Γ; here we focus on $\Gamma \sim 1$.

2. BOLGIANO LENGTH SCALE AND DIFFICULTIES IN REALIZING BO59 SCALING

2.1. Bolgiano Length Scale

The first step in judging whether BO59 scaling is possible is to determine the Bolgiano length L_B from Equation 6. Assuming spatial homogeneity, one can do this based on rigorous relations, within the approximations of the Boussinesq equation (see, e.g., Shraiman & Siggia 1990),

$$\epsilon_u \equiv \langle \nu(\partial_i u_j(\boldsymbol{x}, t))^2 \rangle_{V,t} = \frac{\nu^3}{L^4}(\mathrm{Nu} - 1)\mathrm{RaPr}^{-2}, \tag{7}$$

$$\varepsilon_\theta \equiv \langle \kappa(\partial_i \theta(\boldsymbol{x}, t))^2 \rangle_{V,t} = \kappa \frac{\Delta^2}{L^2} \mathrm{Nu}, \tag{8}$$

for the volume and time-averaged kinetic and thermal dissipation rates, respectively. Here $\mathrm{Ra} = \beta g \Delta L^3/(\nu\kappa)$ and $\mathrm{Pr} = \nu/\kappa$ are the Rayleigh and Prandtl numbers, with Δ the applied temperature difference, and ν and κ the kinematic viscosity and the thermal diffusivity, respectively. For $Nu \gg 1$, these relations imply

$$L_B/L \approx \mathrm{Nu}^{1/2}/(\mathrm{PrRa})^{1/4}. \tag{9}$$

Assuming the large-Ra power law $\mathrm{Nu} \sim \mathrm{Ra}^{1/3}$, which follows from Grossmann & Lohse's (2000) theory and is consistent with the experimental data of Niemela et al. (2000), Nikolaenko et al. (2005), and Niemela & Sreenivasan (2006), one obtains

$$L_B/L \sim \mathrm{Ra}^{-1/12}\mathrm{Pr}^{-1/4}, \tag{10}$$

giving hope that at least for very large Ra and large Pr a separation of scales between L_B and L may arise.

However, Relation 9 and the above argumentation are extremely misleading, as the SFs and the energy and thermal dissipation rates should be locally defined (i.e., as function of $\boldsymbol{x}$), whereas Equation 9 is a global relation. Therefore, one must consider local Bolgiano lengths

$$L_B(\boldsymbol{x}) = \epsilon_u^{5/4}(\boldsymbol{x})\epsilon_\theta^{-3/4}(\boldsymbol{x})(\beta g)^{-3/2}. \tag{11}$$

This quantity became only recently accessible, thanks to local multiple probe measurements (e.g., see He & Tong 2009, He et al. 2007, Wittmer et al. 1998) and in particular to the advancement of numerical simulations (reviewed in Ahlers et al. 2009). **Figure 3** reveals the very strong inhomogeneity of the kinetic and thermal dissipations rates, which of course is not surprising, given the boundary conditions of the flow. The strong peaks of the time-averaged energy dissipation rate $\epsilon_u(\boldsymbol{x})$ at all boundaries reflect the no-slip boundary condition. In contrast, the time-averaged

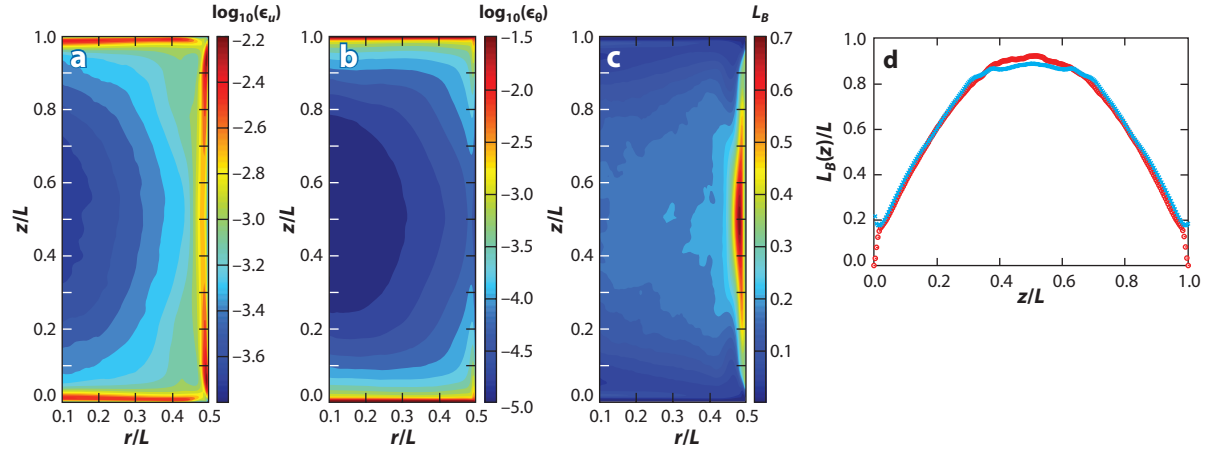

Figure 3

(*a*) Energy dissipation rate $\epsilon_u(\boldsymbol{x})$, (*b*) thermal dissipation rate $\epsilon_\theta(\boldsymbol{x})$, and (*c*) Bolgiano length $L_B(\boldsymbol{x})$, all obtained from the numerical simulations of Kunnen et al. (2008) in a cylindrical cell with $\Gamma = 1$, $\mathrm{Ra} = 10^9$, and $\mathrm{Pr} = 6.4$. (*d*) Vertical profile of $L_B(z)$, as obtained from the numerical simulations of Calzavarini et al. (2002) with periodic boundary conditions in the horizontal direction with $\mathrm{Ra} = 3.5 \times 10^7$ and $\mathrm{Pr} = 1$. Here, $L_B(z)$ has been obtained in two independent ways: by means of Equation 11 (*red circles*) and by evaluating $\epsilon_u r$ and $\beta g r \cdot S_{\theta u_3}(r)$ (the two terms on the right-hand side of Equation 18) and determining the (height-dependent) scale when they cross. These scales—multiplied by an appropriate overall prefactor of order unity—are shown as blue crosses.

thermal dissipation rate $\epsilon_\theta(\boldsymbol{x})$ is only peaked at the top and at the bottom wall, where there are strong temperature gradients—at the sidewall there is no peak because of the adiabatic sidewall boundary conditions. The resulting local Bolgiano length (Equation 11) is shown in **Figure 3*c***, again reflecting this strong inhomogeneity. Except close to the plates, where $L_B/L \approx 0.1$, the Bolgiano length scale is not really separated from the outer length scale L. This result was found earlier in Benzi et al.'s (1998) and, with better precision, Calzavarini et al.'s (2002) simulations, which assume periodic boundary conditions in the horizontal direction: In the bulk of the flow, L_B is the same order of magnitude as the height of the cell (see **Figure 3*d***) and no BO59 can be expected. According to these numerical findings, the best chance to observe BO59 is close to the upper and lower plates. Consistent with this finding, in homogeneous RB convection—convection with an imposed vertical temperature gradient and periodic boundary conditions also in the vertical direction (see also Calzavarini et al. 2005, 2006; Lohse & Toschi 2003) so that no boundary layers can develop—Biferale et al. (2003) find $L_B \sim L$ and correspondingly no BO59 scaling at all. The corresponding SFs, including their subleading corrections, are discussed in Section 3.5.

From the global relation (Equation 10), one may expect that the separation of scales will improve for larger Ra, but again the global argument is misleading. When fitting the numerical values for $L_B(\boldsymbol{x})$ between $0.1 < r/L < 0.4$ at half-height in the regime $10^8 \leq \mathrm{Ra} \leq 10^{10}$, Kunnen et al. (2008) obtained the relation $L_B(\boldsymbol{x} \text{ in bulk})/L = 0.024\,\mathrm{Ra}^{0.107\pm0.016}$ with a positive power-law exponent, suggesting that for larger Ra, what would be a potentially small regime of BO59 scaling will vanish altogether. This indeed is found in the experiments of Sun et al. (2006) and Kunnen et al. (2008) (and numerical simulations as well for the latter; see Section 3).

We try to rationalize the positive power-law exponent in $L_B(\boldsymbol{x}\,\text{in bulk})/L = 0.024\,\mathrm{Ra}^{0.107\pm0.016}$. When we take the bulk estimates of the Grossmann-Lohse theory, $\epsilon_u \sim U^3/L$ and $\epsilon_\theta \sim U\Delta^2/L$, we obtain $L_B(\boldsymbol{x}\,\text{in bulk})/L \sim \mathrm{Re}^3\,\mathrm{Pr}^{3/2}/\mathrm{Ra}^{3/2}$. For regime I_u of Grossmann & Lohse's (2000, 2001, 2002, 2004) theory, where one has $\mathrm{Re} \sim \mathrm{Ra}^{1/2}\mathrm{Pr}^{-5/6}$, this would imply $L_B(\boldsymbol{x}\,\text{in bulk})/L \sim \mathrm{Pr}^{-1}$; for regime IV_u with $\mathrm{Re} \sim \mathrm{Ra}^{4/9}\mathrm{Pr}^{-2/3}$, it would imply $L_B(\boldsymbol{x}\,\text{in bulk})/L \sim \mathrm{Ra}^{-1/6}\,\mathrm{Pr}^{-1/2}$. Neither gives a positive power-law exponent with Ra, for which we therefore do not have any explanation.

2.2. Cascade Picture

Based on Richardson's (1926) cascade picture of turbulence (e.g., see Frisch 1995 for a more modern presentation of this picture), on which Kolmogorov's 1941 theory is based, we now further explain why a realization of BO59 scaling is so difficult, if not impossible. In Kolmogorov's view, the vortices are hierarchically ordered. The relevant energy transport from larger scales to small scales is local in scale, i.e., from scale r to typically scale $r/2$ and from there to scale $r/4$, and so on, down to a scale where viscosity dominates (at the Kolmogorov scale η) (see **Figure 4*a***). The external forcing of homogeneous and isotropic turbulence only takes place at large scales of the order of the size L of the system. The energy input rate e_{in} on the largest scales then equals the transport rate $T_r^u \sim u_r^3/r$ from any scale r in the inertial subrange to scale $r/2$. Here and below, u_r is the typical velocity difference of fluid particles separated over a distance r. In the viscous subrange (i.e., at scales $\sim\eta$ and smaller), the energy is dissipated at a rate ϵ_u, which equals e_{in} because of statistical stationarity. The scale independence of $T_r^u = e_{in} = \epsilon_u$ immediately implies $u_r \sim r^{1/3}$ or Relation 1. The structure of the energy transfer rate $T_r^u \sim u_r^3/r$ is read off from the Navier-Stokes equation, if multiplied by the velocity, by dimensional analysis. Correspondingly, for a passive scalar θ, in the Obukhov-Corrsin picture, the thermal transfer rate $T_r^\theta \sim \theta_r^2 u_r/r$—obtained from multiplying the temperature advection equation with θ—is independent of r and is equal to both the thermal input rate and the thermal dissipation rate ϵ_θ. Together with $u_r \sim r^{1/3}$, this gives $\theta_r \sim r^{1/3}$ or Relation 2.

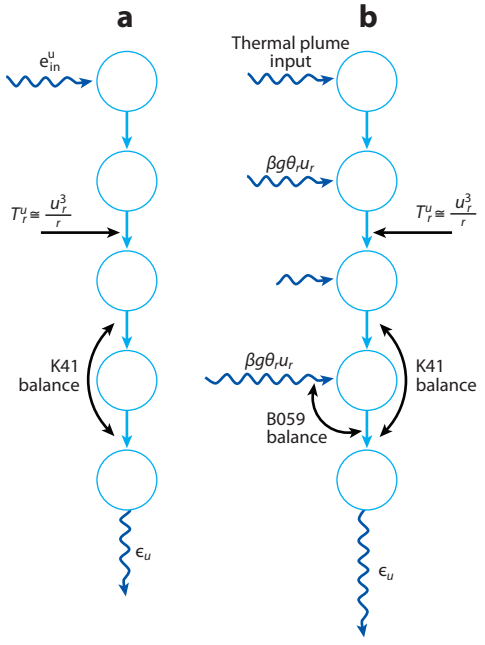

Figure 4

(*a*) Sketch of the Richardson cascade for homogeneous isotropic turbulence. The K41 balance results in the K41 scaling $u_r \sim r^{1/3}$. (*b*) Attempted sketch of the situation in Rayleigh-Bénard flow: On one hand, thermal plumes drive the large-scale convection roll. On the other hand, the buoyancy term $\beta g\theta_r u_r$, whose r dependency is not a priori known, supplies kinetic energy on scale r. Both the K41 and the BO59 balances are shown. If the cascade is downscale, the energy transfer term T_r^u transports the sum of all energies that have been put into the various scales from L to r down the cascade.

What changes for an active scalar θ, i.e., in RB convection, where the underlying equations are now the Oberbeck-Boussinesq equations (Landau & Lifshitz 1987)

$$\partial_t u_i + u_j \partial_j u_i = -\partial_i p + \nu \partial_j^2 u_i + \beta g \delta_{i3} \theta, \tag{12}$$

$$\partial_t \theta + u_j \partial_j \theta = \kappa \partial_j^2 \theta, \tag{13}$$

together with the incompressibility conditions $\partial_i u_i = 0$? [Here $p(\boldsymbol{x}, t)$ is kinematic pressure; scaling-wise the corresponding term $\partial_i p$ has the same structure as the advection term $u_j \partial_j u_i$.] The thermal balance does not change; i.e., $T_r^\theta \sim \theta_r^2 u_r / r \sim \epsilon_\theta$ remains scale-independent. The situation is rather different for the kinetic balance. On one hand, a large-scale convection roll develops, which was first described by Krishnamurti & Howard (1981). It is fed and driven by the small-scale thermal plumes detaching from the boundary layers, as nicely sketched by Kadanoff (2001). This implies an interaction that is scale-wise nonlocal. On the other hand, the large-scale convection roll decays to smaller vortices, so energy is also transported from the large scales toward the small scales. We try to sketch the situation in **Figure 4*b***.

If one wanted to obtain BO59 scaling within the cascade picture, the balance $\beta g\theta_r u_r \sim T_r^u \sim u_r^3/r$ would be required for all scales in the inertial subrange for the energy equation. Indeed, from this balance, together with above thermal balance $T_r^\theta \sim \epsilon_\theta$, one immediately obtains BO59 scaling. However, this would imply that $T_{2r}^u \ll T_r^u$, as on scale r the energy gain from larger scales would be required to be neglible as compared to the energy input through buoyancy $\beta g\theta_r u_r$ on scale r. It therefore would imply that $\beta g\theta_r u_r \gg \beta g\theta_{2r} u_{2r}$ for all scale r in the inertial range. Employing the

framework of Effinger & Grossmann's (1987) mean field theory, Procaccia & Zeitak (1989, 1990) made these assumptions, obtaining BO59 scaling. Similarly, in the framework of shell models (e.g., see Biferale 2003), such balances were also implemented by Brandenburg (1992), Ching & Cheng (2008), Ching & Ko (2008), and Ching et al. (2008a,b), again giving BO59 scaling. Grossmann & L'vov (1993) discuss these balances in Fourier space.

However, within the cascade picture, it is impossible to fulfill the conditions $T^u_{2r} \ll T^u_r$ and $\beta g \theta_r u_r \gg \beta g \theta_{2r} u_{2r}$ over many scales r in the inertial range. Instead, the energy input through buoyancy from the outer length scale L down to the length scale r will accumulate, and the relevant balance on scale r is

$$T^u_r \sim u_r^3/r \sim \sum_{r'=r}^{r'=L} \beta g \theta_{r'} u_{r'}. \tag{14}$$

When assuming some power-law scaling for $\theta_r u_r$ with some positive exponent—e.g., with 4/5 as suggested by the BO59 scaling relation (Equation 5) itself—the sum $\sum_{r'=r}^{r'=L} \beta g \theta_{r'} u_{r'} \sim L^{4/5} + (L/2)^{4/5} + (L/4)^{4/5} + \cdots + r^{4/5}$ in this balance is then a quickly converging geometric series because $r \ll L$. In particular, it quickly becomes independent of r, resulting in K41 scaling. This illustrates the paradoxical nature of the BO59 scaling. Within the framework of the reduced wave vector set approximation (see Eggers & Grossmann 1991, Grossmann & Lohse 1992a), Grossmann & Lohse (1991) indeed found the balance (Equation 14) to dynamically establish, giving basically K41 scaling and $L_B \sim L$. Only when locally injecting, with decreasing scale, an increasing amount of kinetic energy into the cascade—somehow mimicking the kinetic driving of the plumes detaching from the boundary layers—were Grossmann & Lohse (1992b) able to achieve a scaling less steep than K41 for θ_r—but for u_r, no scaling steeper than K41 could be achieved.

2.3. Further Obstacles in Identifying BO59 Scaling

Apart from the inhomogeneity of the flow and the unavoidable limited separation of the length scales between L_B and L, there are further obstacles in identifying BO59 scaling. As pointed out by Lohse (1994), a clear identification of the, at most, short BO59 regime (as shown above) is further complicated by the proximity of the exponents for the BO59 scaling and for the scaling in shear flows. Moreover, because of the large-scale convection roll, there is considerable shear in the RB flow field, making it strongly nonhomogeneous and anisotropic. Either from dimensional analysis (Grossmann et al. 1994, Kuznetsov & L'vov 1981, Lohse 1994, Lohse & Müller-Groeling 1996, Lumley 1967, Tennekes & Lumley 1972) or from a more systematic SO(3) decomposition of the velocity field (e.g., see Arad et al. 1998, 1999a,b; von der Heydt et al. 2001; and Biferale & Procaccia 2005 for a recent review), one obtains for shear flow either dominantly or subdominantly

$$S_u(r) \sim \epsilon_u^{2/3} L_s^{-2/3} r^{4/3}, \tag{15}$$

$$S_\theta(r) \sim \epsilon_\theta \epsilon_u^{-1/3} L_s^{1/3} r^{1/3}, \tag{16}$$

where $L_s \sim \epsilon_u^{1/2}/s^{3/2}$ is the shear length scale and s the typical shear rate. In Fourier space, the corresponding spectra for the kinetic energy and the thermal fluctuations are $E_u(k) \sim \epsilon_u^{2/3} L_s^{-2/3} k^{-7/3}$ and $E_\theta(k) \sim \epsilon_\theta \epsilon_u^{-1/3} L_s^{1/3} k^{-4/3}$, respectively. We note that this type of scaling has been observed in various shear flows, although often only as an anisotropic correction to the (isotropic) K41 scaling. Experimental and numerical examples for the kinetic energy spectrum include Arad et al. 1998, Biferale & Toschi 2001, Biferale et al. 2002b, Kurien & Sreenivasan 2000, and Saddoughi & Veeravalli 1994—for a review, we again refer the reader to Biferale & Procaccia (2005)—and Sreenivasan (1991) gives an example for the temperature fluctuation spectrum. Indeed, close to

the top and bottom plates, Kunnen et al. (2008, their figure 18) find a shear spectrum $S_u(r) \sim r^{4/3}$ for the second-order SF of the vertical velocity.

A proper analysis of the flow properties clearly requires one to disentangle the shear effects and thermal effects, with the help of the SO(3) decompositions, as has been attempted for RB turbulence (Biferale et al. 2003, Rincon 2006). For the longitudinal p-th order velocity SF $S_u^{(p)}(\boldsymbol{r}) = \langle (\boldsymbol{u}(\boldsymbol{x}+\boldsymbol{r}) - \boldsymbol{u}(\boldsymbol{x})) \cdot \boldsymbol{r}/r)^p \rangle_{\boldsymbol{x},t}$, the SO(3) decomposition reads

$$S_u^{(p)}(\boldsymbol{r}) = \sum_{j=0}^{\infty} \sum_{m=-j}^{m=j} S_{jm}^{(p)}(r) Y_{jm}(\boldsymbol{r}/r), \tag{17}$$

where $Y_{jm}(\boldsymbol{r}/r)$ is the spherical harmonics (see Biferale & Procaccia 2005). The projections $S_{jm}^{(p)}$ on the different anisotropic sectors are expected to scale with an m-independent exponent, $S_{jm}^{(p)} \sim r^{\zeta_u^j(p)}$. Yakhot (1992) has generalized the von Kármán–Howarth equation (see Monin & Yaglom 1975) to the case of thermally driven turbulence, obtaining

$$S_u^{(3)}(r) \sim \epsilon r + \beta g r \boldsymbol{e}_z \cdot S_{\theta u_3}(r). \tag{18}$$

Here $\boldsymbol{e}_z$ is the unit vector in the vertical direction, and for simplicity we have suppressed the tensorial structure. The first term on the right-hand side is isotropic ($j = 0$), whereas in the second term, the $j = 1$ factor $\beta g r \boldsymbol{e}_z$ couples to $S_{\theta u_3}(r)$ with its $j = 1, 3, \ldots$ contributions, giving projections on all sectors $j = 0, 1, 2, \ldots$. Biferale et al. (2003) point out that the dimensional isotropic balance in the $j = 0$ sector reads $S_u^{(3),\, j=0}(r) \sim \epsilon r + \beta g r \boldsymbol{e}_z S_{\theta u_3}^{j=1}(r)$, with the second term being subdominant, implying K41-type scaling, whereas in the anisotropic sectors $j > 0$, one obtains

$$S_u^{(3),j}(r) \sim \beta g r \boldsymbol{e}_z S_{\theta u_3}^{j-1}(r). \tag{19}$$

Relation 19 reveals that it is the anisotropic contribution of the third-order velocity SF that, according to the BO59 dimensional argument, should balance the buoyancy term. In Section 3.5, we report Biferale et al.'s (2003) numerical results on homogeneous RB convection, showing that Relation 19 does not hold. The clean SO(3) analysis of Biferale et al. (2003) was possible only because the authors restricted themselves to the kind of artificial case of homogeneous RB flow, i.e., the case with an imposed vertical temperature gradient, but without any walls. In real RB flow, walls are present, and close to the walls, the SO(3) analysis must be replaced by an SO(2) analysis, as done by Biferale et al. (2002b) for shear flow. We do not further discuss this complication here.

Apart from the SO(3) decomposition [or close to walls, SO(2)], another helpful tool for data analysis may be the property of extended self-similarity (ESS), as first found by Benzi et al. (1993). The method, plotting (logarithms of) SFs of different orders p against each other and not against the scale r, is usually effective in revealing mutual scaling relations and in particular intermittency. In the context of RB convection, it has first been applied by Benzi et al. (1994) and later by Cioni et al. (1995), Ching (2000), Zhou & Xia (2001), Skrbek et al. (2002), Ching et al. (2003b), and Kunnen et al. (2008). Independent of the scaling of the second-order velocity SF (K41, BO59, shear flow scaling), dimensional scaling implies $S_u^{(p)}(r) \sim (S_u^{(2)}(r))^{p/2}$. However, even for homogeneous and isotropic flows, there are major deviations from this dimensional scaling—the so-called intermittency corrections (see Frisch 1995, Ishihara et al. 2009, Sreenivasan & Antonia 1997 for reviews). Such intermittency corrections are also present in RB flow for both the velocity and the temperature SFs (see Berschadskii et al. 2004; Ching 2000; Ching & Cheng 2008; Ching et al. 2003b, 2008a; Sun et al. 2006; Zhang & Wu 2005). Disentangling the anisotropic effects and intermittency effects (Biferale & Toschi 2001, Biferale et al. 2002a, Toschi et al. 1999) and effects from the buoyancy-driven mechanism remains a major challenge.

We would like to stress that even if the above-mentioned complications (e.g., shear, intermittency) were overcome, the intrinsic difficulties of the BO59 scaling as discussed in Section 2.2 still remain.

3. TEMPERATURE AND VELOCITY SPECTRA AND STRUCTURE FUNCTIONS

3.1. Overview of Main Experimental Methods

Above we discuss the theoretical difficulties in detecting BO59 scaling, namely anisotropy, inhomogeneity, intermittency, and the lack of a wide inertial range that can provide a sufficient separation of the relevant length scales (η, L_B, L_s, and L). However, in addition there is also a lack of suitable experimental techniques for direct and high-resolution simultaneous multipoint measurements of the velocity and temperature fields.

By far most experimental studies on temperature and velocity fluctuations employ only point measurements, resulting in temperature and velocity time series acquired at a single point in the convection cell. At best, such measurements are performed at several locations in the flow. The basic methods at hand are thermometry or bolometry for the temperature time series and later laser Doppler velocimetry (LDV) for the velocity time series. To connect the time-domain results to the theoretical predictions made for the spatial domain, investigators invoke Taylor's (1938) frozen-flow hypothesis, either explicitly or implicitly. The validity of this hypothesis requires that turbulent velocity fluctuations are much smaller than the mean flow velocity. However, the mean velocity is approximately zero in the central region of the convection cell and is comparable to the root-mean-square (rms) velocity near the sidewall and plate regions (Qiu et al. 2000, Sun et al. 2005, Xia et al. 2003). Therefore, the condition for the Taylor hypothesis is often not met in turbulent RB convection, and its applicability to the system is at best doubtful. Nonetheless, we discuss results from such point measurements in Sections 3.2 and 3.3.

Only recently, with the maturing of PIV (see Adrian 1991) and other similar techniques for the full velocity field measurement, have the experimental limitations of single-point measurements become less of a problem. We discuss the results of recent PIV measurements of the velocity field in RB convection in Section 3.4. Finally, the numerical results on temperature and velocity spectra and SFs are reviewed in Section 3.5. Here, the full spatial information is available, but Ra is limited.

3.2. Time-Domain Measurements

The first systematic measurements in turbulent RB convection by Libchaber and coworkers (Castaing et al. 1989, Heslot et al. 1987, Procaccia et al. 1991, Sano et al. 1989, Wu et al. 1990) were restricted to temperature time series, from which temperature frequency power spectra were obtained through Fourier transformation. These temperature power spectra, and also those based on later temperature time-series measurements at $\mathrm{Pr} \approx 0.7$ and larger, display a scaling exponent around -1.3 ± 0.1 (e.g., Procaccia et al. 1991) to -1.4 (e.g., Wu et al. 1990), similar to the BO59 value $-7/5$ (but also similar to the shear spectrum value $-4/3$). In contrast, low-Pr liquid metals (such as mercury, $\mathrm{Pr} \approx 0.025$) show more complicated behavior, depending on the value of Ra. We first discuss experiments made in fluids with $\mathrm{Pr} \geq 0.7$.

Libchaber and coworkers' early experiments (Castaing et al. 1989, Heslot et al. 1987, Procaccia et al. 1991, Sano et al. 1989, Wu et al. 1990; reviewed in Siggia 1994) used low-temperature helium gas as the working fluid and measured temperature frequency power spectra with miniaturized semiconductor bolometers placed inside the convection cell. Wu et al.'s (1990) experiments were

made in a $\Gamma = 0.5$ cylindrical cell with Ra spanning from 7×10^6 to 4×10^{14}. Their main result is that up to[1] at least $\mathrm{Ra} = 7 \times 10^{10}$, the temperature power spectra exhibit a universal shape characterized by a power-law range in the low-frequency region and an exponential decay in the high-frequency tails, which is characteristic of dissipation range behavior. All power spectra can be collapsed onto a single curve by a simple rescaling of power density and frequency, i.e., shifts in log-log plot. A slope of -1.4 was observed in the low-frequency power-law region, and the authors noted that the scaling range increases with increasing Ra, starting from $\mathrm{Ra} \sim 10^8$, where the scaling range is almost zero. Interestingly, Wu et al. (1990) did not take the finding of the exponent -1.4 in the temperature power spectra as indicative of the existence of BO59 scaling; rather they seem to regard this as a mere coincidence. Instead, their main message is that a kind of universality may exist in the cascades of turbulent fluctuations in the dissipative region of thermal turbulence. Wu et al. (1990) suggested that this may represent a generalization of Kolmogorov's picture of turbulence; i.e., a lack of universality in the original Kolmogorov spirit may be restored by a proper multifractal transformation, which is referred to as a multifractal universality (Frisch 1995). In their experiment, Wu et al. measured temperature at the cell center, where the convective flow may be regarded as homogeneous but the mean flow is essentially zero, and the authors themselves point out that Taylor's frozen-flow hypothesis is not believed to be applicable. We shall take the same view when discussing below the other experiments conducted under similar circumstances.

Whereas Wu et al. (1990) focused primarily on whether the temperature power spectra has a universal shape, Chilla et al. (1993) studied both the shape and the scaling properties of the power spectra and SFs of the temperature field. Their experiment was carried out in a rectangular cell using water as the convecting fluid, with $\mathrm{Pr} \approx 4$ and Ra between 10^6 and 4×10^8. The 2D temperature field was measured using a laser sweeping technique in which the deflection of the laser beam is proportional to the local temperature gradient averaged along the beam path (Rubio et al. 1989). The temperature was then reconstructed by integrating the measured temperature gradient. Because the measured temperature gradient was integrated along the optical path of the laser beam, this technique required that the flow field be mainly 2D. These authors also used a thermocouple placed inside the fluid to measure the local temperature. Their results show that wave-number power spectra of the temperature from the laser sweeping method and the frequency power spectra measured by the thermocouple have similar shape. In fact these two types of spectra largely overlap when normalized properly. The authors suggest that this coincidence may be taken as an indirect verification of Taylor's frozen-flow hypothesis (actually a modified version of it because it involved averaged quantities), although they also conceded that it did not constitute a rigorous proof of the hypothesis. Using the spatially averaged temperature field, they also studied low-order SFs. In a later study, Cioni et al. (1995), employing ESS, found consistency of Chilla et al.'s (1993) results with BO59.

Several later studies focused primarily on the scaling of the power spectra. For example, in a helium gas experiment, Niemela et al. (2000) reported observing both BO59- and K41-type scaling in the frequency power spectrum obtained from measured temperature time series. However, as seen from **Figure 5*a***, for both regimes the scaling range is less than a decade, and it is not known whether the power spectrum remains the same shape at the high end of Ra that was reached in

[1]The transition at $\mathrm{Ra} \approx 7 \times 10^{10}$, which Wu et al. (1990) and later Procaccia et al. (1991) found in various quantities—including the temperature spectra themselves—has consistently been interpreted to be caused by temperature-fluctuation averaging effects around the bolometer (Grossmann & Lohse 1993). Although already Siggia (1994) favors Grossmann & Lohse (1993)'s interpretation, it has not been strictly proven. Due to space limitations, we do not further discuss this issue in this review.

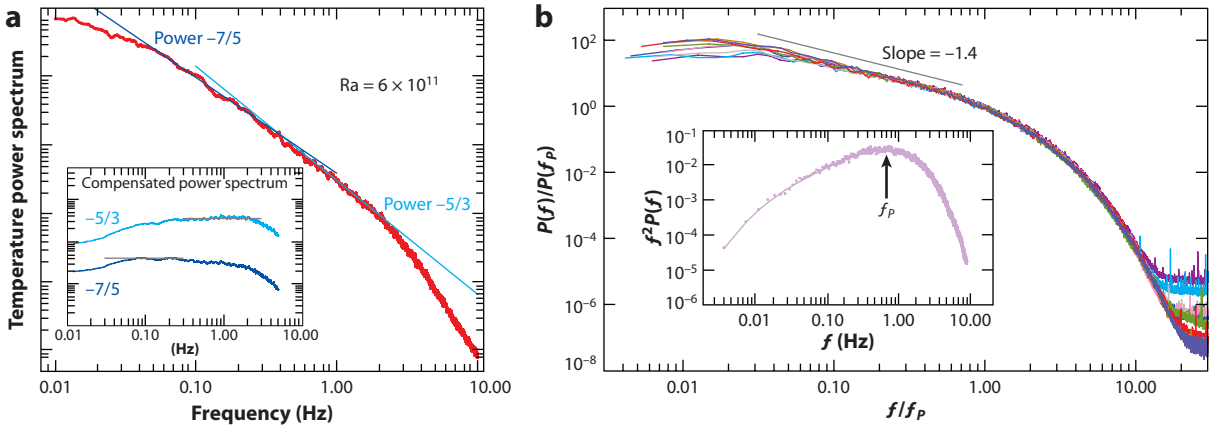

Figure 5

(*a*) Frequency power spectrum of temperature measured in the center of an $\Gamma = 0.5$ cylinder filled with helium (Pr = 0.7) at Ra = 6×10^{11}. (*Inset*) The K41- and BO59-compensated spectra. Figure taken from Niemela et al. 2000. (*b*) Frequency power spectra of temperature measured in water (Pr = 4.3) with Ra from 2×10^9 to 1.3×10^{11}. Measurements were made at the center of cylindrical cells of $\Gamma = 1$ and 0.5. Spectra are presented after a simple scaling by the peak frequency f_p [and $P(f_p)$] of the temperature dissipation spectra $f^2P(f)$; an example of the latter is shown in the inset of the figure. Figure adapted from Zhou & Xia 2001.

their experiment ($\sim 10^{17}$); it is also unclear why the spectra that Wu et al. (1990) measured under similar conditions (Ra, Pr, Γ) showed only a single scaling exponent. Skrbek et al. (2002), using the same apparatus as Niemela et al. (2000) but with $\Gamma = 1$, measured local temperature in helium at Ra = 1.5×10^{11} near the sidewall. Their SFs obtained directly from the temperature time series did not show a reasonable scaling range, so the authors resorted to the ESS method, which yielded good scaling behavior. As the ESS can only give relative scaling exponents, it is not possible to distinguish between BO59 and K41 scaling behaviors (at least for lower orders).

Ashkenazi & Steinberg (1999) conducted a convection experiment in a rectangular box of aspect ratio 0.7, with sulfur hexafluoride (SF_6) gas as the convecting fluid. By working near the gas-liquid critical point of SF_6, one can vary the Rayleigh and Prandtl numbers of this system over a wide range, Ra from 10^9 to 10^{14} and Pr from 1 to 300, although at the price of having pronounced non-Boussinesq effects at the edge of this domain. Using the scattering produced by the critical density fluctuations, Ashkenazi & Steinberg (1999) measured the local velocity with a modified LDV technique (Lukaschuk et al. 2001). Their measured frequency power spectra of the vertical velocity exhibit power-law scaling, and the fitted exponent averaged over various values of Ra and Pr is −2.4, which is close to the BO59 value of −11/5 predicted for the wave-number spectra. They also measured the local temperature fluctuations at both the cell center and near the sidewall by placing small thermistors in the fluid, observing an interesting feature in the measured temperature frequency power spectra. Even for Ra up to 5×10^{12} and Pr less than 50, the measured spectra did not show a noticeable scaling range. But for Pr from 90 to 300 and Ra from 8×10^{13} to 3×10^{14}, the measured spectra exhibited about one decade of scaling with a fitted exponent of −1.45. Another interesting feature of Ashkenazi & Steinberg's (1999) experiment is their construction of the velocity and temperature cross-spectra using the measured time series of the two quantities at the same location (although it is not clear how far the temperature probe is separated from the LDV measuring volume). They reported a scaling exponent of −1.85 for the obtained cross-spectrum, which is close to the theoretical value −9/5 predicted for the BO59 scaling, i.e., the Fourier transform of Equation 5.

In a convection experiment in water, Zhou & Xia (2001) measured local temperature fluctuations in cylindrical cells of aspect ratio 1 and 0.5, with Ra varying from 4×10^8 to 1×10^{11} while maintaining Pr $\sim$ 4. Most of their measurements were made at the cell center, but for one Ra (1.85×10^{10}), they scanned the position from the bottom plate to the center. Both the power spectra and SFs were investigated from the measured temperature time series. Extending an idea first introduced in the wave-number domain by She & Jackson (1993), that the peak wave-number k_p of the dissipation spectrum $k^2E(k)$ can be used as a characteristic scale to collapse the energy spectrum $E(k)$, Zhou & Xia (2001) found that a simple scaling of the form $P(f)/P(f_p)$ versus f/f_p could collapse all measured frequency temperature power spectra $P(f)$, with f_p the peak frequency of the temperature dissipation spectrum $f^2P(f)$. As seen from **Figure 5*b***, all spectra with Ra $> 1 \times 10^{10}$ exhibit a well-defined scaling range with an exponent of -1.4 (the inset of the figure shows an example of the dissipation spectrum). In contrast to the method used by Wu et al. (1990), this simple scaling does not need any adjustable phenomenological parameters. In addition, Zhou & Xia did not observe a change of the spectra shape around Ra $\simeq 7 \times 10^{10}$ as found by Wu et al. (1990). The simple scaling using the peak frequency of the dissipation spectra as the characteristic scale to collapse frequency power spectra was later found to be also applicable to velocity. Using LDV, Shang & Xia (2001) measured the vertical velocity in a cylindrical cell filled with water. They found that the simple scaling method works well for velocity frequency power spectra measured near the sidewall over the range of Ra from 10^8 to 10^{10}.

Whereas most of the temperature measurements in the time domain made at Pr $\geq$ 0.7 show scaling behavior with an exponent close to the expected BO59 value, the behavior in low-Pr liquid metal appears to be different. This is in coincidence with the theoretical expectation from Equation 10: Smaller Pr should result in larger L_B and thus a more pronounced K41 scaling regime and a less pronounced BO59 scaling regime. Cioni et al. (1995) made a comparative study of local temperature fluctuations in both water (Pr $\sim$ 7) and mercury (Pr $= 0.025$). They used a cylindrical cell of aspect ratio one, and made the measurements above the center of the bottom plate at a distance of one-quarter of the cell height. For water, the temperature frequency power spectrum has a slope of -1.4 (Ra $\sim 10^{10}$). For mercury, a rather short and curved scaling range (which actually straddles the Bolgiano frequency $f_B = U/L_B$) of the spectrum (at Ra $\sim 10^9$) may be fitted with an exponent -1.63, which is close to the Kolmogorov scaling. Using Taylor's hypothesis, Cioni et al. (1995) then studied the corresponding temperature spatial SFs, which showed no scaling behavior. When using the ESS analysis, they found that relative scaling exponents are consistent with those found for passive scalars in homogeneous and isotropic turbulence. Based on the temperature time-series measurements from both water and mercury, Cioni et al. (1995) concluded that temperature in bulk RB convection behaves as a passive scalar for the low-Pr case with power-law exponents close to the K41 value, whereas for Pr $\sim$ 1, the exponents are close to the BO59 value. They further attributed this to the difference in the Bolgiano scale for the two cases, as, according to Equation 10, at least the global L_B depends on Pr. This conclusion appears to be supported by Takeshita et al. (1996), who studied mercury convection over the range $10^6 <$ Ra $< 10^8$. Their measured temperature frequency power spectra are similar to those found by Cioni et al. (1995), i.e., a limited scaling range with f_B straddled in the middle. To shed light on the force balances in the bulk, Takeshita et al. (1996) estimated, based on the measured temperature fluctuations and velocity, that the buoyancy force is only approximately 1% of the inertial force in the central region of the cell interior. This again suggests that the temperature behaves like a passive scalar in this parameter range. In a later experiment by the same group (Glazier et al. 1999), a much higher Ra ($\sim 5 \times 10^{10}$) is reached. Because of the very low Pr, the corresponding Reynolds number is approximately $\sim 5 \times 10^5$, much higher than those reached at high-Pr fluids. Indeed, the measured temperature frequency power spectrum shows a wider scaling range than

previous cases, and the estimated f_B is well above the noise cutoff frequency. But even in this case, the fitted exponent (−1.47) still differs from the BO59 prediction.

Although extremely important for the BO59 scaling, the force balance relation $\beta g \theta_r u_r \sim u_r^3/r$ has not been directly tested experimentally, and only a few indirect tests exist. Using a generalized ESS scheme, Ching (2000) analyzed the Chicago data measured in the cell center in terms of the normalized temperature temporal SFs and found the existence of two scaling regimes separated by the Bolgiano timescale $\tau_B = L_B/U$. Using velocity data from a numerical study (Benzi et al. 1996) and the Chicago temperature data, Ching (2000) also tested the force balance (in the time domain) and found that it does not hold. In a later study of simultaneous velocity and temperature data measured in water (Shang et al. 2003), both in the time domain, Ching et al. (2004a) found the existence of cross-scaling between the normalized velocity and temperature SFs measured in the cell center; i.e., when plotting one against the other on log-log scale, a linear relation emerges, whereas none exhibited scaling behavior on its own. However, as shown in **Figure 6**, the cross-scaling exponent is different from that implied by the BO59 force balance, thus, again, not supporting BO59 scaling. We stress that the above cross-scaling exists only for timescales above τ_B (indicated in **Figure 6**), which Ching et al. (2004a) found to be a buoyancy-relevant scale from the cross-correlation function between the increments of the vertical velocity and of temperature; i.e., a strong correlation exists between the two increments above τ_B but not below it. Similar properties have recently been found to exist also between the temperature and concentration fields in turbulent convection (Zhou & Xia 2008). Thus, although the BO59 scaling itself is not supported, there does exist a range of scales above which buoyancy is important, and that may be termed the Bolgiano regime.

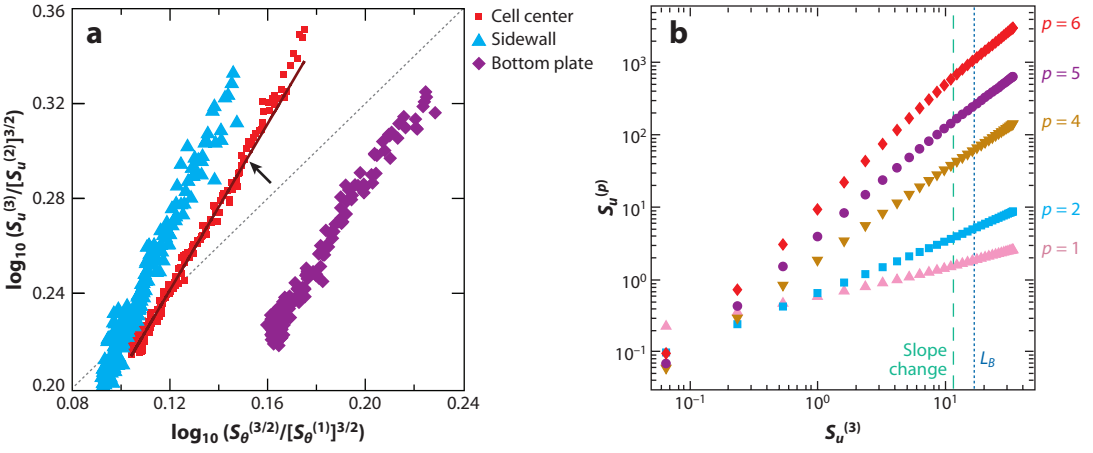

Figure 6

Extended self-similarity plot of (*a*) time structure functions (SFs) and (*b*) space SFs. (*a*) $\log(S_u^{(3)}(\tau)/[S_u^{(2)}]^{3/2}(\tau))$ versus $\log(S_\theta^{(3/2)}(\tau)/[S_\theta^{(1)}]^{3/2}(\tau))$ measured at the cell center (*red squares*). The solid line (implying cross-scaling between the two quantities) is a least-squares fit to the data points in the Bolgiano regime (indicated by the *arrow*, representing τ_B) but is plotted for the whole range of τ. Results for measurements taken near the sidewall (*blue triangles*) and the bottom plate (*purple diamonds*) are also shown, but for which the cross-scaling is less certain. The dotted line has slope 1, which is implied by the Bolgiano scaling. Figure adapted from Ching et al. 2004a. (*b*) $\log S_{u_3}^{(p)}(r)$ versus $\log S_{u_3}^{(3)}(r)$ from the numerical simulations of Kunnen et al. (2008) at $\mathrm{Ra} = 1.11 \times 10^8$ with $p = 1, 2, 4, 5$, and 6, from bottom to top. The dotted line indicates the local L_B estimate. At the dashed line, a slope change is found in all curves. Figure adapted from Kunnen et al. 2008.

3.3. Converting Time-Domain Data into Space-Domain Data Using Local Taylor Hypothesis

As mentioned above, because of the absence of a sufficiently large mean flow, the conditions for Taylor's frozen-flow hypothesis are not satisfied in most parts of the convection cell. This in turn raises serious questions regarding the interpretation of results from time-domain measurements. However, as the direct real-space measurement techniques such as PIV cannot be used conveniently in fluids such as gas and liquid metal, time-domain measurement will continue to play an important role. It is therefore highly desirable to be able to connect time or frequency domain data with spatial domain theoretical predictions in a meaningful way. The standard Taylor hypothesis assumes that velocity time series can be converted into spatial series according to $v(x = Ut) \equiv v(t)$, where the mean flow velocity U should be much larger than the rms velocity. When this condition is not met, the so-called local Taylor hypothesis may be used (e.g., see Tennekes & Lumley 1972). Sun et al. (2006) recently applied one such method, introduced by Pinton & Labbé (1994), to turbulent RB convection. By assuming that small-scale structures in the inertial range are advected by large eddies at the integral scale, Pinton & Labbé (1994) propose that the velocity $v(x)$ at location x should be related to the velocity $v(t)$ by $x = \int_0^t \bar{v}(\tau)d\tau$, where $\bar{v}(\tau)$ is a local running average of $v(t)$ over the integral timescale T_{int}, $\bar{v}(\tau) = T_{\text{int}}^{-1} \int_{\tau - T_{\text{int}}/2}^{\tau + T_{\text{int}}/2} v(t)dt$.

To test this method, Pinton & Labbé (1994) used hot-wire data from swirling flows and found that for both the velocity power spectrum and the SF, the corrected spatial domain data exhibit a longer scaling range and an exponent closer to the predicted value (K41) than those obtained with time-domain data. Recently, Sun et al. (2006) applied this method to turbulent convection. They used velocity time series measured with the LDV technique by Shang & Xia (2001) and compared it with their own PIV data measured under similar conditions. They used the large-eddy turnover time of the system as T_{int} to convert $v(t)$ into $v(x)$. As shown in **Figure 7**, compared with the SF calculated with the time domain, the space-domain SF is similar to that from the PIV data in terms of both the slope and the scaling range. After correcting with the local Taylor method, the space-domain data clearly exhibit a longer scaling range that moreover sets in near the expected

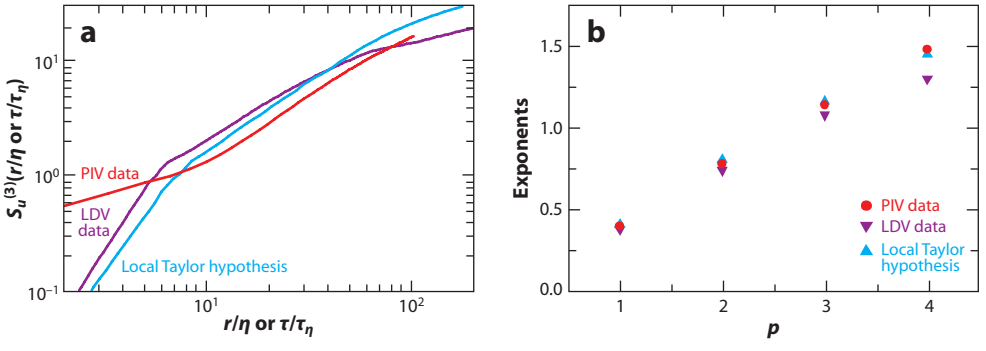

Figure 7

(*a*) Third-order longitudinal velocity structure functions (SFs) (based on the modulus) calculated from time-domain laser Doppler velocimetry (LDV) data (*purple*), LDV data converted into space-domain data using the local Taylor hypothesis (*blue*), and particle image velocimetry (PIV) data (*red*). Their slopes in the scaling range are 1.08, 1.16, and 1.14, respectively. The vertical velocities used were measured near the sidewall of aspect-ratio-one cylindrical cells filled with water (Ra $= 7 \times 10^9$ and Pr $= 4.3$). The spatial resolution of the PIV measurement is approximately 1.6η, which is not enough to resolve dissipative range scales, which presumably leads to the too large PIV-measured structure function at small scales. (*b*) Exponents of the three types of SFs as in panel *a*, for orders 1 to 4; the symbol colors correspond to those in panel *a*. Data taken from Shang & Xia 2001 and Sun et al. 2006.

scale $r \approx 10\eta$. The difference between the time-domain and space-domain SFs becomes larger at larger-order p, and thus with increasing order of the SF, the correction becomes more important. It is clear from these results that corrections to the time-domain data can be quite significant even in the presence of a relatively strong mean flow (the LDV data were measured near the sidewall of the convection cell, where the large-scale flow mean velocity $\bar{v} = 11.7$ mm s^{-1} and the rms velocity $v_{rms} = 6.5$ mm s^{-1}). Clearly the local Taylor hypothesis can be used to effectively convert time-domain velocity series into spatial series in situations in which the usual condition for the conventional Taylor hypothesis is not satisfied; i.e., the mean flow either is absent or is comparable to the rms velocity. However, without velocity data, this method cannot be applied to convert the temperature time series, which is more readily available and can be more conveniently measured in thermal convection. Therefore, it is highly desirable to directly study SF, which indeed has been done in recent years thanks to the developments in PIV.

3.4. Space-Domain Measurements

To our knowledge, the first spatial-domain measurements of velocity differences in turbulent thermal convection were made by Tong & Shen (1992). Using the technique of homodyne photon-correlation spectroscopy, they measured velocity differences of particle pairs in a scattering volume of linear dimension r in an aspect-ratio-one cylindrical cell filled with water. Their results show that $u_r \sim r^{0.6}$ over about a decade of r and for $5 \times 10^7 \leq \mathrm{Ra} \leq 10^{10}$. Thus, their results appear to agree with the BO59 prediction for the first-order velocity SF. However, they should be interpreted with caution. The measured photon-correlation function records differences in the Doppler shifts of all particle pairs in the scattering volume of size ℓ, with separations from zero up to ℓ (ℓ varied in the experiment and was taken as r). Therefore, the measured u_r is essentially an integration of velocity differences of particles with separations from 0 to r. Another space-domain measurement of the velocity field was made in mercury by Mashiko et al. (2004). Using the same apparatus as Glazier et al. (1999), the authors measured the vertical velocity profile along the cylindrical axis of the cell by the technique of ultrasonic velocimetry. Their wave-number energy spectrum at $\mathrm{Ra} = 5 \times 10^{10}$ (at the cell center) showed about a decade of power-law behavior with an exponent consistent with the BO59 value of $-11/5$. They also computed the velocity SFs and found that the second-order SF compensated by $r^{6/5}$ showed a very small scaling range consistent with BO59. We note that Mashiko et al. (2004) used a mode decomposition method to separate the slow dynamics related to the mean flow and the fast dynamics related to the turbulent cascades and that in the calculation of their energy spectra and SFs, mean flow and several low-order modes were subtracted. It is thus clear that, although both Tong & Shen (1992) and Mashiko et al. (2004) found some evidence for BO59-like scaling, no direct spatial velocity SFs have been measured. Additionally, no direct spatial temperature SFs have been measured in the studies discussed above. Obviously, both velocity and temperature should be in the same class of scaling behavior (either K41, BO59, or shear-flow scaling), over the same range of scales, and under the same conditions if we are to agree on an acceptable and convincing cascade dynamics.

In an attempt to determine the cascades of both temperature and velocity variances in turbulent thermal convection, Sun et al. (2006) made high-resolution multipoint measurements of both the velocity and the temperature fields in water, using a cylindrical cell of aspect ratio one ($\mathrm{Ra} \approx 1.0 \times 10^{10}$ and $\mathrm{Pr} = 4.3$). Using PIV and the multi-thermistor-probe technique, these authors measured the 2D velocity field and the temperature difference along the vertical direction, from which they obtained the real-space longitudinal and transverse SFs for both the horizontal and vertical velocity components and spatial temperature SFs, respectively. The spatial resolutions

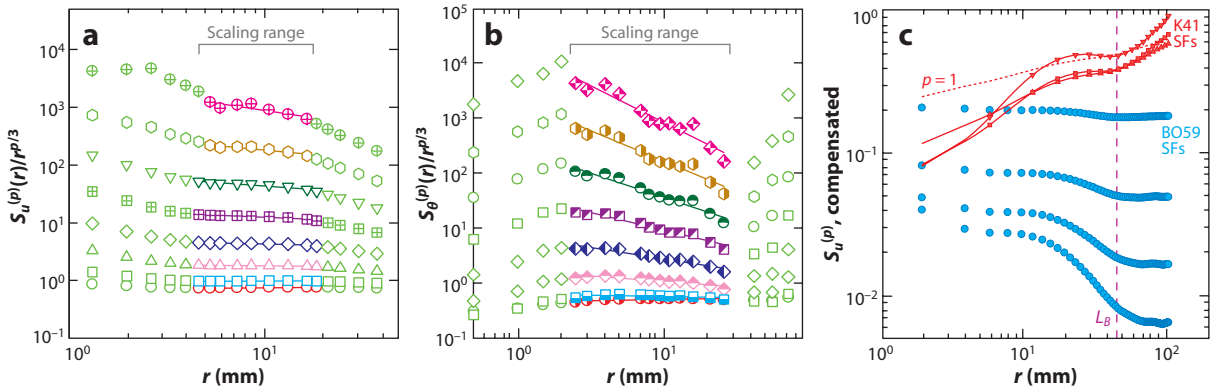

Figure 8

(*a*,*b*) Compensated real-space velocity and temperature structure functions (SFs) of order 1 to 8 (*from bottom to top*) measured at the central region of an aspect-ratio-unity cylindrical cell filled with water (Ra $\sim 1 \times 10^{10}$ and Pr $= 4.3$). Data inside and outside the scaling range are represented by different colors, and the lines represent power-law fits to data in the inertial range. Figure taken from Sun et al. 2006. (*c*) Compensated transverse SFs of the vertical velocity measured near the cell center in a cylindrical cell (Ra $= 1.1 \times 10^9$, Pr $= 6.37$, and $\Gamma = 1$). Blue circles represent BO59-compensated SFs, and lines represent K41-compensated SFs. The order p increases from 1 to 4 from top to bottom for BO59. The red dotted line is the $p = 1$ SF with K41 compensation. Similarly, lines with triangles, squares, and upside-down triangles represent $p = 2$, 3, and 4, respectively. The estimated local L_B is indicated by the purple dashed line. Figure taken from Kunnen et al. 2008.

in both the velocity and temperature measurements are comparable to the Kolmogorov scale and are approximately 10 times smaller than the global Bolgiano scale, so the inertial-range features are well-resolved. An important aspect of this study is that for all orders $p = 1$ to $p = 8$, both the velocity and temperature SFs exhibit their respective scaling behavior over the same range of scales. An example of the real-space velocity and temperature SFs (compensated by K41 predictions) measured in the central region of the convection cell is shown in **Figure 8*a*,*b***. These SFs show a high level of convergence even at order 8, as evidenced by their integration kernels (Sun et al. 2006). The power-law fits to data are in the inertial range $10\eta \leq r \leq \mathcal{L}$, where the Kolmogorov scale is $\eta \approx 0.4$ mm, and $\mathcal{L} \approx 30$ mm is the integral length obtained by integrating the longitudinal velocity autocorrelation function. The global quantity-based Bolgiano scale in this case is $L_B \approx 5$ mm. Thus the entire inertial range should be above L_B. Nonetheless, these results clearly show that the low-order SFs are closer to K41 behavior. Deviations become progressively larger with increasing order, presumably because of intermittency effects, which can be described by the hierarchy models of She & Lévêque (1994) for velocity and of Ruiz-Chavarria et al. (1996) for passive scalars. **Figure 9*a*** shows exponents of both longitudinal and transverse velocity SFs and of temperature SFs, and their comparisons with various model predictions. The results show convincingly that for both the temperature and the velocity fields, in the inertial range and for orders 1 to 8 consistently, the cascades of the temperature and velocity fluctuations in the cell center do not obey the BO59 scaling. Instead, K41-type scalings with intermittency properly taken into account can well describe the observed scaling behavior. Thus in the cell center, both velocity and temperature exhibit the same scaling behavior that one would find for the velocity and for a passive scalar in homogeneous and isotropic Navier-Stokes turbulence. However, in the sidewall region, Sun et al. (2006) found that, whereas the SFs of horizontal velocity are consistent with those in the central region, the exponents for the vertical velocity and temperature are different from those in the central region and do not follow BO59, K41, or She & Lévêque's (1994) model predictions. By considering the co-action of buoyancy and inertial forces and using dimensional

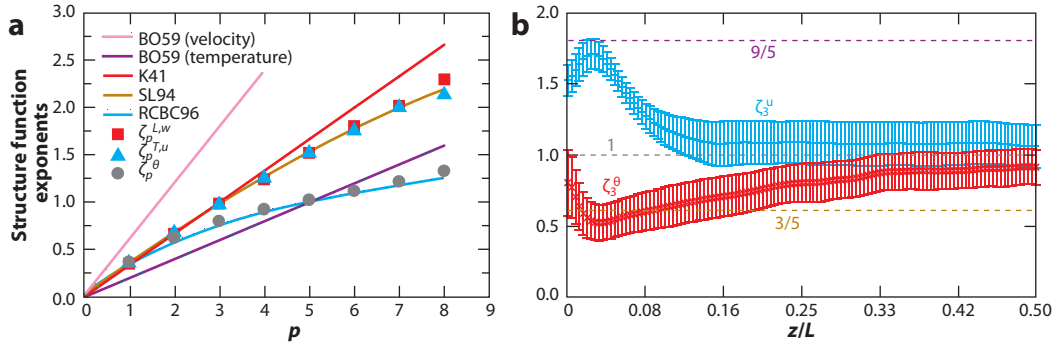

Figure 9

(*a*) Exponents of structure functions (SFs) measured at the center of an aspect-ratio-unity cylindrical cell filled with water (Ra $\sim 1 \times 10^{10}$ and Pr $= 4.3$). Here $\zeta_p^{L,w}$ is the exponent of the p-th-order longitudinal SF of the vertical velocity, $\zeta_p^{T,u}$ is that of the transverse SF of the horizontal velocity, and ζ_p^{θ} is the exponent of the temperature SF. The pink and purple lines represent BO59 predictions for velocity and temperature, respectively; the red line represents K41 and OC (Obukhov-Corrsin) predictions for velocity and passive scalar; and the gold and blue lines represent, respectively, values resulting from the hierarchical model of She & Lévêque (1994) for the velocity and of Ruiz-Chavarria et al. (1996) for the passive scalar, both with appropriately chosen parameters. Figure adapted from Sun et al. 2006. (*b*) Scaling exponents ζ_3^u and ζ_3^{θ} as a function of the distance z/L from the plate, at Ra $= 3.5 \times 10^7$ and Pr $= 1$, based on numerical simulations with periodic boundary conditions in the horizontal direction. The scaling exponents are measured in an r regime where extended self-similarity holds. Figure adapted from Calzavarini et al. 2002.

analysis, Sun et al. (2006) found $S_u^{(p)} \sim r^{2p/5}$ and $S_\theta^{(p)} \sim r^{3p/10}$, which agree with the measured low-order SFs (as intermittency is not considered, the dimensional analysis is not expected to be correct for higher-order SFs). In a later investigation of the velocity field in the central region of the same cell, Zhou et al. (2008) made a systematic test of the local homogeneity and isotropy using a number of criteria. Their results show that homogeneity and isotropy hold to an excellent degree in the central region of the RB cell, which suggests that the effect of buoyancy is negligible on small-scale turbulence in the central region. They attribute this to the fact that in aspect-ratio-unity cells, the large-scale circulation carries most of the thermal plumes along the perimeter of the system, so there are few plumes passing through the central region.

Recently, Kunnen et al. (2008) also measured spatial velocity SFs based on the stereoscopic PIV technique. The experiment was done in water (Pr $= 6.37$) in the regime $1.1 \times 10^8 \leq \text{Ra} \leq 1.1 \times 10^9$. From their numerical result (discussed in Section 3.5), the local Bolgiano scale (Equation 11), shown in **Figure 3*c***, was known. In the center, for which the SFs are reported, and for Ra $= 1.1 \times 10^8$, it is approximately 1/5 of the external length scale L, but it grows to approximately $L/3$ at Ra $= 1.1 \times 10^9$. Between L_B and L, the BO59 compensated second-order velocity SFs (i.e., the SFs divided by $r^{6/5}$) indeed give a straight line (see **Figure 8*c***), but the range is rather limited and shrinks with rising Ra. Clearly, there is no extended BO59 scaling. Close to the plates, Kunnen et al. (2008) reveal the shear scaling (Equation 15) in the second-order velocity SF. As pointed out by Kunnen et al. (2008), their results and those of Sun et al. (2006) are in fact complementary to each other, despite the seeming contradiction, as shown in **Figure 8**. The key properties here are the local Bolgiano scale and the size of the measurement area. According to their numerical result, the local Bolgiano scale in Sun et al.'s (2006) case (Ra $= 1.0 \times 10^{10}$) equals $L_B \approx 56$ mm, rather than $\approx$5 mm as estimated from global quantities. Sun et al.'s (2006) measurement area is 40×40 mm^2; thus K41-like behavior is expected for their measurement in the cell center. To verify this experimentally, one would need to measure local energy and thermal dissipation rates (and hence local L_B).

Kunnen et al. (2008) also applied ESS, plotting the p-th order velocity SF against $S_u^{(3)}$; the relative scaling exponent is called ξ_p, defined by $S_u^{(p)}(r) \sim (S_u^{(3)}(r))^{\xi_p}$. Two regimes can be identified (see **Figure 6*b***): For $r \leq L_B/2$, the relative exponents ξ_p resemble the ones one would expect for intermittency-corrected K41 scaling and that are well described by She & Lévêque's (1994) model (e.g., $\xi_6 = 1.78$). For $r \geq L_B/2$, the ξ_p are smaller and Ra-dependent, however, with an error bar within the range of what has been found by Toschi et al. (1999) for the ξ_p in channel-flow turbulence (e.g., $\xi_6 = 1.44$).

Zhou et al. (2008) measured the velocity circulation SFs in the central region of the RB system. Their result shows that the circulation SFs also exhibit K41-like behavior, but they are more sensitive to local anisotropy than the velocity field itself. These results give further support to Sun et al.'s (2006) findings that in the central region of the RB system, K41-like rather than BO59-like dynamics prevails. Putting together results from these two studies, we see the emergence of a consistent picture regarding the cascades of turbulent velocity and temperature fluctuations; i.e., for the directly measured SFs, no BO59-like behavior is observed in turbulent RB convection.

3.5. Structure Functions and Spectra From Numerical Simulations

The tremendous advantage of numerical simulations of RB flow is that in principle all data are available. However, due to computational costs, only limited Ra and Pr can be achieved, and only in the past 15 years or so have turbulent 3D RB simulations become possible. For a more detailed discussion, we refer the reader to the review by Ahlers et al. (2009).

Kerr (1996) provides one of the first numerical simulations for really turbulent RB convection, achieving $\mathrm{Ra} = 2 \times 10^7$ at $\mathrm{Pr} = 0.7$ with periodic boundary conditions at the sidewalls. He finds about one decade of K41-type scaling $E_u(k) \sim k^{-5/3}$ and less steep scaling for the temperature spectrum, consistent with $E_\theta(k) \sim k^{-1}$, both inconsistent with the BO59 picture.

Calzavarini et al. (2002) provide a numerical simulation in a similar Ra and Pr regime with a Lattice-Boltzmann scheme. The SFs do not scale. However, some scaling regimes can be identified in ESS plots of the SFs against each other. When measuring the local scaling exponents $\zeta_u^{(p)}$ and $\zeta_\theta^{(p)}$ in the respective SFs for that ESS scaling regime as a function of the distance z from the plates, they obtain values consistent with K41 scaling in the bulk, where $L_B(z) \sim L$, and values consistent with BO59 scaling close to the plates, where $L_B(z) \approx 0.2L$ (see **Figure 9*b*** for the local scaling exponents and **Figure 3*c*** for the corresponding local Bolgiano scale).

Camussi & Verzicco (1998) provide temperature and velocity frequency spectra for RB flow in mercury at $\Gamma = 1/2$ and $\mathrm{Pr} = 0.022$ and for $5 \times 10^4 \leq \mathrm{Ra} \leq 10^6$, based on their numerical simulations. To allow for a one-to-one comparison, they calculated the spectra from velocity and temperature time series taken at the cell center and close to the cell wall. No indication of BO59 scaling was reported. Moreover, Camussi & Verzicco (2004) employed numerical time series to calculate spectra and SFs $S_u(\tau)$ and $S_\theta(\tau)$, but now for $\mathrm{Pr} = 0.7$ and for Ra up to 2×10^{11}. The temperature frequency spectrum showed a power-law exponent close to $-5/3$ (K41) in the center and close to $-7/5$ (BO59) at mid-height close to the sidewall, where $S_\theta(\tau)$ showed the corresponding slope 2/5. Depending on the position and velocity component, the velocity frequency spectrum showed either a slope close to $-5/3$, or even a less steep slope (smaller modulus of slope)—in fact similar to the value $-7/5$ of the temperature frequency spectrum—but clearly no indication of BO59 scaling. Rincon (2006) performed numerical simulations at $\mathrm{Ra} = 10^6$, $\mathrm{Pr} = 1$, and $\Gamma = 5$, employing the SO(3) analysis to properly treat isotropic and anisotropic projections of the SF tensor. However, the Rayleigh number in these simulations is too small to reveal any scaling, and the focus of the paper is on energy balances resulting from the Boussinesq

equations. The paper again stresses the importance of disentangling anisotropy, inhomogeneity, and buoyancy effects.

The hitherto most complete numerical calculations of real-space velocity and temperature SFs were performed by Kunnen et al. (2008). For the velocity SFs in the center of the cell, they found similar results as those obtained from their stereoscopical PIV measurements, including the relative ESS scaling exponents. In particular, with increasing Ra, the BO59 regime becomes even less limited, which is consistent with the trend in the local Bolgiano length. In the small regime beyond $r > L_B$ (less than half a decade even for the best case Ra $= 10^8$), the BO59-compensated temperature spectra are more horizontal than the K41-compensated ones, although both show an unexplained increase at the very large scales, $r \approx L$. With increasing Ra, this regime becomes even smaller.

All the numerical simulations reported above in this subsection are for the flow in real cells with no-slip boundary conditions, at least at the top and bottom walls, leading to inhomogeneities in the flow. As discussed in Section 2.3, the inhomogeneities can be avoided in the so-called homogeneous RB flow. Biferale et al. (2003) applied the SO(3) decomposition for this type of flow. They not only found K41 scaling (with the standard intermittency corrections) in the isotropic $j = 0$ sector, but they also found no evidence for BO59 scaling in the subleading, anisotropic $j = 1$ sector: The BO59 dimensional scaling relation (Equation 19) for $j = 1$ clearly is not fulfilled. Instead, the anisotropic fluctuations in the RB system are anomalous and universal, with similar relative scaling exponents as in random Kolmogorov flow or in other types of shear flows (Toschi et al. 1999).

4. SMALL-SCALE MIXING OF ACTIVE AND PASSIVE SCALARS

In Grossmann & Lohse's (2000, 2001, 2002, 2004) theory, the kinetic energy and thermal dissipation rates have been decomposed into boundary layer and bulk contributions, and a laminar Prandtl-Blasius boundary layer, in a time-averaged sense, has been assumed. This theory can successfully describe and predict Nu and Re's dependency on Ra and Pr (e.g., see the recent review in Ahlers et al. 2009). In a recent high-resolution measurement of the properties of the velocity boundary layer, Sun et al. (2008) have found that, despite the intermittent emission of plumes, the Blasius-type laminar boundary condition is indeed a good approximation, in a time-averaged sense, both in terms of its scaling and its various dynamic properties. In the Prandtl-Blasius boundary-layer theory, temperature is treated as a passive scalar, but because of buoyancy, in the inertial range and above the Bolgiano scale, temperature behaves as an active scalar. One naturally wonders what would be the properties of the temperature field at these small scales. Specifically, how does the temperature as an active scalar compare with a passive scalar under the same conditions?

4.1. Small-Scale Anisotropy of the Temperature Field

The persistence of nonzero skewness of the scalar derivatives is a hallmark of passive scalar mixing, as it invalidates the local isotropy assumption of the classical Kolmogorov-Obukhov-Corrsin theory of passive scalars (Sreenivasan 1991). The nonzero skewness is believed to result from sharp fronts or gradients of the scalar. By examining the skewness $S_\theta \equiv S(\theta) \equiv \langle(\theta - \langle\theta\rangle)^3\rangle / \langle(\theta - \langle\theta\rangle)^2\rangle^{3/2}$ of the temperature and the skewness $S_{\partial_t\theta} \equiv S(\partial_t\theta)$ of its time derivative in thermal convection, Belmonte & Libchaber (1996) studied the small-scale mixing properties of the temperature field, in particular the question of active versus passive. Their experiment was conducted in a cubic cell of aspect ratio one filled with pressurized gas (helium, nitrogen, or sulfur hexafluoride) at room temperature and spanned a range of Ra from 2×10^7 to 1×10^{11} with Pr $= 0.7$. Sharp

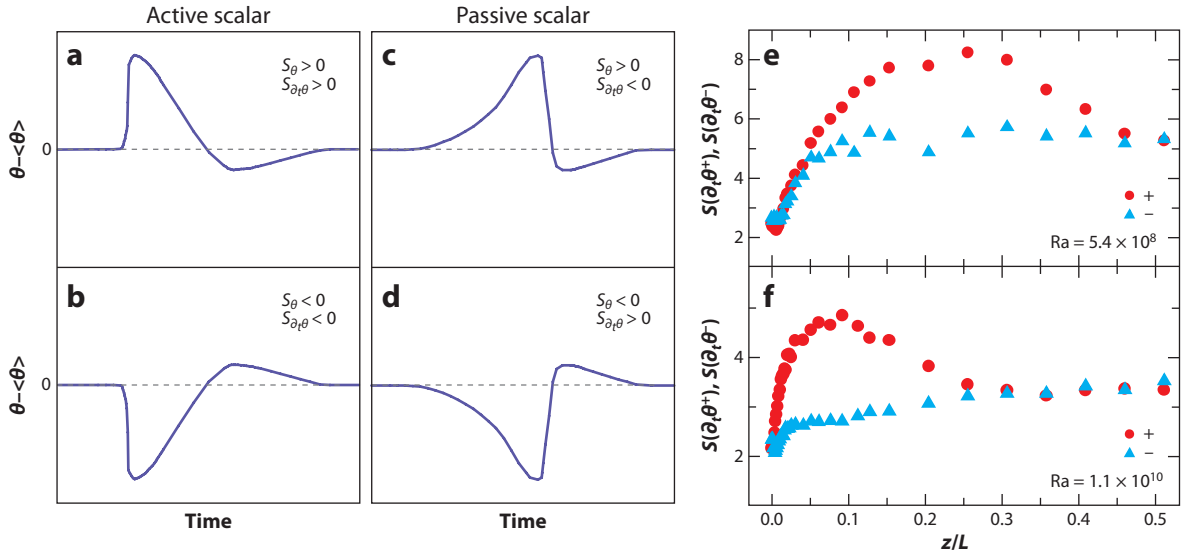

Figure 10

(*a–d*) A sketch of four scenarios of temperature asymmetries (relative to the mean), according to the signs of their skewness S_θ and the skewness $S_{\partial_t\theta}$ of their time derivative. Panels *a* and *b* correspond to an active scalar for which $S_\theta S_{\partial_t\theta} > 0$, and panels *c* and *d* correspond to a passive scalar for which $S_\theta S_{\partial_t\theta} < 0$. Figure adapted from Belmonte & Libchaber 1996. (*e*,*f*) Skewness of the plus (*red circles*) and minus (*blue triangles*) temperature derivative as functions of the scaled distance z/L for two values of Ra. The width of the mixing zone is characterized by the gap in the z direction within which $S(\partial_t\theta^+)$ and $S(\partial_t\theta^-)$ differ from each other. Figure taken from Zhou & Xia 2002.

fronts in passive scalars manifest themselves as ramp-cliff (slow rise and fast decay) structures in the time series, which would produce positive S_θ and negative $S_{\partial_t\theta}$ when the passive scalar is temperature measured near a mildly heated plate (Sreenivasan & Antonia 1977). Extending this to active scalars, Belmonte & Libchaber (1996) argued that, when measured near the hot plate in thermal convection, temperature time series would possess cliff-ramp structures that would give rise to positive S_θ and $S_{\partial_t\theta}$. These cliff-ramp structures are believed to be associated with plumes. Based on this, Belmonte & Libchaber (1996) classified four different scenarios according to the signs of S_θ and $S_{\partial_t\theta}$. As shown in **Figure 10**, passive and active scalars produced at the hot and cold plates (corresponding to hot and cold plumes for the active case) can be identified by the sign of the product of $S_\theta S_{\partial_t\theta}$. Belmonte & Libchaber's (1996) measured profile $S_{\partial_t\theta}(z)$ from the cold plate is mostly negative outside the boundary layer, so they concluded that the temperature is active. Moreover, they argued that the region over which $S_{\partial_t\theta}$ remains negative corresponds to the mixing zone but did not quantify this further. In a recent study of temperature fluctuations measured inside the conducting plates of the convection cell, Sun & Xia (2007) found that indeed the product of $S_\theta S_{\partial_t\theta}$ is positive in both the cold and hot plates and can be described by the power-law $\mathrm{Ra}^{0.22}$ over the range 5×10^7–1×10^{11}, which may be taken as a quantitative measure of the increased strength of plume eruptions.

Emran & Schumacher (2008) analyzed the skewness of the temperature and its spatial derivative (in vertical direction) numerically, up to $\mathrm{Ra} = 10^9$, always finding non-Gaussian probability density functions (PDFs) of the temperature statistics. In contrast, the statistics for the spatial derivative of the temperature is similar to that of a passive scalar. In the bulk, $S_{\partial_z\theta}$ decreases with increasing Ra. Moreover, profiles $S_\theta(z)$ are provided, but none for $S_{\partial_t\theta}(z)$, so that a classification of the regimes according to Belmonte & Libchaber (1996) is not possible.

In a somewhat different approach, Zhou & Xia (2002) studied the skewness of the so-called plus and minus temperature increments $\theta_\tau^\pm = (|\theta_\tau| \pm \theta_\tau)/2$, where $\theta_\tau = \theta(t+\tau) - \theta(t)$ is the temperature increment over a time interval τ. [Plus and minus increments were first used in the study of ramp structures in the velocity field in Navier-Stokes turbulence (Vainshtein & Sreenivasan 1994) and later in the context of the temperature field by Aivalis et al. (2004).] When a (hot) plume passes through a temperature probe, it would produce a spike with a steep rising edge (due to its cap) and a relatively gentle falling edge (due to its tail) in the measured time series. The plus and minus temperature increments thus capture, respectively, the slope of the rising and falling edges for τ smaller than the size of a plume (in the time domain). Therefore, in regions where hot plumes dominate over cold ones, θ_τ^+ would be expected to be larger than θ_τ^-, and vice versa in regions where cold plumes dominate. Indeed, Zhou & Xia found that for $\tau < \tau_B = L_B/U$, the skewness $S(\theta_\tau^+) > S(\theta_\tau^-)$ in regions where hot plumes dominate. This also suggests that the cap thickness (in time domain) of a typical plume should be smaller than τ_B but larger than τ_η. For $\tau > \tau_B$, features smaller than the corresponding scale are averaged out, resulting in the same values for the plus and minus skewness. Zhou & Xia (2002) also found that $S(\partial_t\theta^+)$ and $S(\partial_t\theta^-)$ are the same in the boundary layer and central regions of the cell but differ in regions where plumes dominate, which is shown in the right panel of **Figure 10** for two values of Ra. The width (in the z direction) of the region in which the two quantities differ shrinks as Ra increases, which in fact has a scaling exponent as that predicted for the width of the mixing zone (Castaing et al. 1989). The mixing zone plays an important role in the Chicago model for hard turbulence (Castaing et al. 1989), and the plus and minus skewness provides a useful definition for its quantitative characterization. Recently, it has been found that quantities such as the profile of vorticity fluctuations (Zhou et al. 2007) and skewness of spatial temperature gradient and local thermal dissipation rate (He & Tong 2009) can all be used to characterize the mixing zone.

4.2. Comparative Studies of Active and Passive Scalars

A fascinating property of passive scalars is the saturation of the scaling exponent of their high-order SFs; i.e., the exponent ζ_p^θ approaches a constant ζ_∞^θ for large enough order p. The saturation is believed to be related to the ramp-cliff structures (or fronts) in the scalar (Celani et al. 2000, Moisy et al. 2001). With the temperature time series in thermal convection found to exhibit cliff-ramp structures (Belmonte & Libchaber 1996, Zhou & Xia 2002), it is natural to ask whether the temperature field as an active scalar would possess the saturation property. In a 2D numerical study of thermal convection, Celani et al. (2001) found that the temperature indeed exhibits saturation phenomenon. Experimentally, Zhou & Xia (2002) measured long time records (consisting of 1.2×10^8 data points, corresponding to 37,000 large-eddy turnover times) of local temperature both near the sidewall region and at the center in an aspect-ratio-one cylindrical cell filled with water ($\mathrm{Ra} = 1.8 \times 10^{10}$, $\mathrm{Pr} = 4$). As the high-order moments are dominated by large temperature excursions, the saturation of the SF exponent is equivalent to the scaled PDF $r^{-\zeta_\infty^\theta} P(\theta_r)$ becoming independent of r for inertial range values of $\theta_r \gg \theta_{rms}$. Because high-order SFs are very sensitive to the far tails of the PDF, collapsing of the scaled PDF is a statistically more reliable test of the saturation (Celani et al. 2000, 2001). By examining both the scaled PDF $\tau^{-\zeta_\infty^\theta} P(\delta_\tau)$ of temperature increments over varying timescales in the inertial range and the cumulated probability $\int_{\theta_\tau}^{\infty} P(\delta_\tau) d\delta_\tau$, Zhou & Xia found evidence for the saturation of the temperature SFs near the sidewalls, but not at the cell center. Because plumes are abundant at the sidewall but scarce in the center, this finding suggests that the saturation is caused by the presence of plumes. As mentioned in Section 3.2, Skrbek et al. (2002) analyzed temperature time series measured in helium ($\mathrm{Ra} = 1.5 \times 10^{11}$), also near the sidewall, using the ESS method. They find no saturation of the ESS (relative) scaling exponents

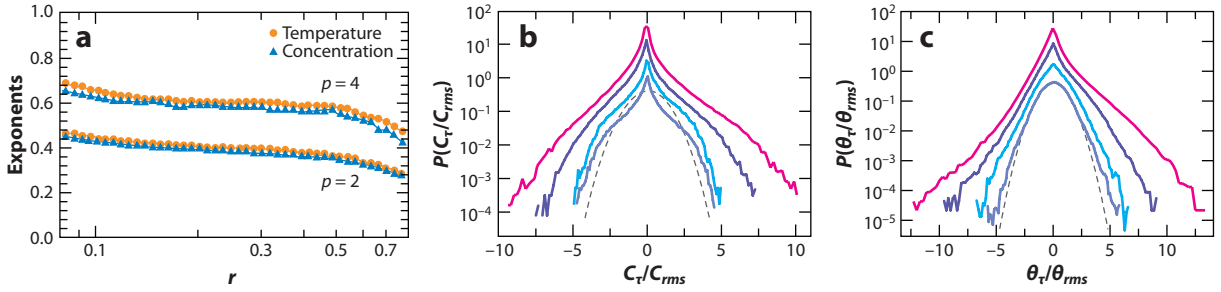

Figure 11

(*a*) Local scaling exponents of temperature (*circles*) and concentration (*triangles*) structure functions for orders 2 and 4, from 2D simulations made at Ra $= 10^7$. Figure taken from Celani et al. 2002. (*b*,*c*) Probability density functions of concentration and temperature increments normalized by their standard deviations for four time intervals (*from top to bottom*): $\tau/\tau_B = 0.05$, 0.15, 1, and 10. The curves have been shifted vertically for clarity, and the gray dashed curve indicates a Gaussian distribution of variance 1. Measurements were made near the sidewall, at mid-height, of a rectangular cell filled with water (Ra $= 1.2 \times 10^{10}$ and Pr $= 5.3$). Figure taken from Zhou & Xia 2008.

ξ_p^θ with increasing order, up to $p = 16$. However, from that result it cannot be concluded that the scaling exponents ζ_p^θ of the temperature SFs do not saturate either.

A fruitful way to investigate the temperature field with respect to the question of whether it behaves more as an active or more as a passive scalar in thermal convection would be to make a direct comparative study with a real passive scalar (such as the concentration of a dispersed dye) under the same conditions. Such an approach has been taken mostly in numerical studies. Celani et al. (2002) investigated the scaling properties of both the temperature and a passive scalar governed by the Boussinesq equations in a 2D numerical study and found that the two scalar fields have the same even-order SF exponents, as shown in **Figure 11**. They conjectured that this may be attributed to the existence of so-called statistically preserved structures in the temperature field, as is the case for passive scalars. In a shell model study of thermal convection, Ching et al. (2002, 2003a) found numerical evidence that the equivalence of even-order statistics of active and passive scalars can indeed be understood from the presence of statistically preserved structures.

On the experimental side, there exist only a few comparative studies of active and passive scalars advected by the same flow. Using liquid crystal imaging and planar laser-induced fluorescence techniques, Gluckman et al. (1993) studied the geometric properties of isothermal and isoconcentration contours in turbulent convection in water (Ra $\sim 10^7$–10^8). They found that the isoconcentration contours show a limited fractal scaling range. In contrast, the isotherms do not exhibit fractal scaling, which does not support Procaccia et al.'s (1991) suggestion that the temperature field appears fractal above a certain scale. Conversely, the local curvature of both the isoconcentration and isothermal contours possesses a stretched exponential PDF with asymmetric tails. By injecting a fluorescent dye into a rectangular cell filled with water, Zhou & Xia (2008) made simultaneous and separate measurements of the local temperature, using a small thermistor, and dye-concentration fluctuations, using laser-induced fluorescence, in close proximity (near the sidewall at mid-height). They showed that although the two scalars are advected by the same turbulent flow, the quantities themselves and their small-scale increments distribute differently. Below τ_B, the temperature behaves as a passive scalar, and above τ_B it behaves as an active scalar, where it also possesses a higher level of intermittency as compared with the passive scalar (dye concentration). **Figure 11*b*,*c*** plots the PDF of concentration and temperature increments over several time intervals, respectively. The PDFs of temperature increments change from non-Gaussian in small scales to near Gaussian in large scales, whereas those of concentration increments remain

non-Gaussian for all scales investigated; i.e., as τ changes from small to large scales, the shapes of the concentration-increment PDFs are more similar among themselves than those of the temperature, and hence the passive scalar is less intermittent than the active one. The finding that an active scalar is more intermittent than a passive one is consistent with the saturation of the SF exponent for the temperature. The saturation exponent ζ_∞^θ is found to be 0.8 for an active scalar from experiment (Zhou & Xia 2002) and 2D simulations (Celani et al. 2001) and 1.45 for a passive scalar measured in a swirling flow (Moisy et al. 2001). This suggests that ζ_∞^θ deviates more from the dimensional predictions for active scalars than passive ones, implying that the active scalar is more intermittent. As a possible future experiment, the saturation of both active and passive scalars advected by the same flow should be measured.

As a closing remark, we point out that many of the studies reviewed in this section are made in the time domain; therefore, they also face the question regarding the validity of the Taylor hypothesis, and one should always bear this in mind when interpreting the results and connecting them to theoretical predictions.

5. CONCLUSIONS AND OUTLOOK

The discussions in this review reflect that the issue regarding the nature of cascades of the velocity and temperature fluctuations in turbulent thermal convection is not fully settled. On one hand, both temperature and temperature gradient PDFs and their skewnesses and force balances on large scales carry the feature of an active scalar, pronouncedly different from those of a passive scalar like a concentration field. On the other hand, BO59 scaling has not been found over a large range of scales and many hints point toward the sketch of **Figure 2** being unrealistic. According to Kunnen et al. (2008), as the Ra dependency of the local Bolgiano scale $L_B(\mathbf{x})$ is an increasing function of Ra—at least in the center of the cell, where the effect of anisotropy and shear is smallest—future attempts to find BO59 scaling should be made with lower Ra and higher Pr to increase the potential BO59 range, if it exists at all. This, of course, strongly limits the possible inertial scaling regime, again revealing the conflict of requirements for extended BO59 scaling: This fundamental obstacle—the lack of separation of length scales between L and L_B—appears to place conflicting demands on the control parameters of the system, and an extended BO59 scaling regime therefore may never be achieved.

Ultimately, a true test of the Bolgiano argument should consist of observing K41-like scaling, for both velocity and temperature, below L_B. In contrast, above L_B, one should observe BO59-like scaling, again for both velocity and temperature, just as sketched in **Figure 2**. Because the Kolmogorov scale and the local Bolgiano scale have opposite dependency on Ra, this means that simultaneous observation of K41 and BO59 scalings at the same location is unlikely, if not impossible. In light of this, several different approaches may yield fruitful results. The first one is to select an appropriate range of Ra and Pr, and suitable system size and aspect ratio, and look for different scalings in different regions of the convection cell; for example, BO59-like scaling near the boundary layer and K41-like scaling in the cell center. The second approach is to look for different scalings in the same location of the cell by tuning the local L_B to be either larger or smaller than the experimentally accessible scale, which could be achieved by using different working fluids, for example. Attempts along the line of the first approach have been made by Sun et al. (2006) and Kunnen et al. (2008), whereas the second type of approach has not been attempted in a systematic way. A third approach may be to use cells of wider aspect ratio, $\Gamma \gg 1$, to allow for a large length scale at least in the horizontal direction and for a possible separation of scales between L_B and ΓL. For any of these efforts, it will in addition be helpful to employ the SO(3) decomposition of the flow to better disentangle scaling corrections due to shear and

scaling corrections due to buoyancy. Also for future studies, a quantitative test of the force balance relation $\beta g \theta_r u_r \sim u_r^3/r$ in direct spatial measurements of the velocity and temperature fields will need to be made—as done in Calzavarini et al. (2002) for numerical simulations (see **Figure 3*d***).

As pointed out in Section 1, the RB system may be ideal to study turbulence as it is experimentally accessible and as the governing equations and boundary conditions are exactly known. However, thanks to the richness of its dynamics, it clearly is not the easiest system to study clean and extended scaling regimes of SFs over a large range of scales.

DISCLOSURE STATEMENT

The authors are not aware of any affiliations, memberships, funding, or financial holdings that might be perceived as affecting the objectivity of this review.

ACKNOWLEDGMENTS

We thank all our colleagues and collaborators on this subject for various discussions over the past 20 years. We have learned tremendously from them and enjoy and appreciate the joint research efforts to better understand turbulent thermal convection. D.L. acknowledges FOM for the continuous support and K.Q.X. the Hong Kong Research Grants Council (grant nos. CUHK 403806 and 403807).

LITERATURE CITED

Adrian RJ. 1991. Particle-imaging techniques for experimental fluid mechanics. *Annu. Rev. Fluid Mech.* 23:261–304

Ahlers G, Grossmann S, Lohse D. 2009. Heat transfer and large scale dynamics in turbulent Rayleigh-Bénard convection. *Rev. Mod. Phys.* 81:503–37

Aivalis KG, Schumacher J, Sreenivasan KR. 2004. Sign-symmetry of temperature structure functions. *Phys. Rev. E* 69:066315

Arad I, Biferale L, Mazzitelli I, Procaccia I. 1999a. Disentangling scaling properties in anisotropic and inhomogeneous turbulence. *Phys. Rev. Lett.* 82:5040–43

Arad I, Dhruva B, Kurien S, L'vov VS, Procaccia I, Sreenivasan KR. 1998. Extraction of anisotropic contributions in turbulent flows. *Phys. Rev. Lett.* 81:5330–33

Arad I, L'vov V, Procaccia I. 1999b. Correlation functions in isotropic and anisotropic turbulence: the role of the symmetry group. *Phys. Rev. E* 61:6753–65

Arneodo A, Baudet C, Belin F, Benzi R, Castaing B, et al. 1996. Structure functions in turbulence, in various flow configurations, at Reynolds number between 30 and 5000, using extended self-similarity. *Europhys. Lett.* 34:411–16

Ashkenazi S, Steinberg V. 1999. Spectra and statistics of velocity and temperature fluctuations in turbulent convection. *Phys. Rev. Lett.* 83:4760–63

Batchelor GK. 1953. *The Theory of Homogeneous Turbulence*. Cambridge, UK: Cambridge Univ. Press

Belmonte A, Libchaber A. 1996. Thermal signature of plumes in turbulent convection: the skewness of the derivative. *Phys. Rev. E* 53:4893–98

Benzi R, Biferale L, Ciliberto S, Struglia MV, Tripiccione R. 1996. Generalized scaling in fully developed turbulence. *Phys. D* 96:162–81

Benzi R, Ciliberto S, Tripiccione R, Baudet C, Massaioli F, Succi S. 1993. Extended self-similarity in turbulent flows. *Phys. Rev. E* 48:R29–32

Benzi R, Tripiccione R, Massaioli F, Succi S, Ciliberto S. 1994. On the scaling of the velocity and temperature structure functions in Rayleigh-Bénard convection. *Europhys. Lett.* 25:341–46

Benzi R, Toschi F, Tripiccione R. 1998. On the heat transfer in the Rayleigh-Bénard system. *J. Stat. Phys.* 93:901–18

Berschadskii A, Niemela JJ, Praskovsky A, Sreenivasan KR. 2004. Clusterization and intermittency of temperature fluctuations in turbulent convection. *Phys. Rev. E* 69:056314
Biferale L. 2003. Shell models of energy cascade in turbulence. *Annu. Rev. Fluid Mech.* 35:441–68
Biferale L, Calzavarini E, Toschi F, Tripiccione R. 2003. Universality of anisotropic fluctuations from numerical simulations of turbulent flows. *Europhys. Lett.* 64:461–67
Biferale L, Daumont I, Lanotte A, Toschi F. 2002a. Anomalous and dimensional scaling in anisotorpic turbulence. *Phys. Rev. E* 66:056306
Biferale L, Lohse D, Mazzitelli I, Toschi F. 2002b. Probing structures in channel flow through SO(3) and SO(2) decomposition. *J. Fluid Mech.* 452:39–59
Biferale L, Procaccia I. 2005. Anisotropy in turbulent flows and in turbulent transport. *Phys. Rep.* 414:43–164
Biferale L, Toschi F. 2001. Anisotropies in homogeneous turbulence: hierarchy of scaling exponents and intermittency of the anisotropic sectors. *Phys. Rev. Lett.* 86:4831–34
Bolgiano R. 1959. Turbulent spectra in a stably stratified atmosphere. *J. Geophys. Res.* 64:2226–29
Brandenburg A. 1992. Energy spectra in a model for convective turbulence. *Phys. Rev. Lett.* 69:605–8
Calzavarini E, Doering CR, Gibbon JD, Lohse D, Tanabe A, Toschi F. 2006. Exponentially growing solutions of homogeneous Rayleigh-Bénard flow. *Phys. Rev. E* 73:R035301
Calzavarini E, Lohse D, Toschi F, Tripiccione R. 2005. Rayleigh and Prandtl number scaling in the bulk of Rayleigh-Bénard turbulence. *Phys. Fluids* 17:055107
Calzavarini E, Toschi F, Tripiccione R. 2002. Evidences of Bolgiano-Obhukhov scaling in three-dimensional Rayleigh-Bénard convection. *Phys. Rev. E* 66:016304
Camussi R, Verzicco R. 1998. Convective turbulence in mercury: scaling laws and spectra. *Phys. Fluids* 10:516–27
Camussi R, Verzicco R. 2004. Temporal statistics in high Rayleigh number convective turbulence. *Eur. J. Mech. B Fluids* 23:427–42
Cardin P, Olson P. 1994. Chaotic thermal convection in a rapidly rotating spherical shell: consequences for flow in the outer core. *Phys. Earth Planet. Inter.* 82:235–59
Castaing B, Gunaratne G, Heslot F, Kadanoff L, Libchaber A, et al. 1989. Scaling of hard thermal turbulence in Rayleigh-Bénard convection. *J. Fluid Mech.* 204:1–30
Celani A, Lanotte A, Mazzino A, Vergassola M. 2000. Universality and saturation of intermittency in passive scalar turbulence. *Phys. Rev. Lett.* 84:2385–88
Celani A, Matsumoto T, Mazzino A, Vergassola M. 2002. Scaling and universality in turbulent convection. *Phys. Rev. Lett.* 88:054503
Celani A, Mazzino A, Vergassola M. 2001. Thermal plume turbulence. *Phys. Fluids* 13:2133–35
Chilla F, Ciliberto S, Innocenti C, Pampaloni E. 1993. Boundary layer and scaling properties in turbulent thermal convection. *Il Nuovo Cim. D* 15:1229–49
Ching ESC. 2000. Intermittency of temperature field in turbulent convection. *Phys. Rev. E* 61:R33–36
Ching ESC, Cheng WC. 2008. Anomalous scaling and refined similarity of an active scalar in a shell model of homogeneous turbulent convection. *Phys. Rev. E* 77:015303
Ching ESC, Chui KW, Shang XD, Qiu XL, Tong P, Xia KQ. 2004a. Velocity and temperature cross-scaling in turbulent thermal convection. *J. Turbul.* 5:27
Ching ESC, Cohen Y, Gilbert T, Procaccia I. 2002. Statistically preserved structures and anomalous scaling in turbulent active scalar advection. *Europhys. Lett.* 60:369–75
Ching ESC, Cohen Y, Gilbert T, Procaccia I. 2003a. Active and passive fields in turbulent transport: the role of statistically preserved structures. *Phys. Rev. E* 67:016304
Ching ESC, Guo H, Cheng WC. 2008a. Understanding the different scaling behavior in various shell models proposed for turbulent thermal convection. *Phys. D* 237:2009–14
Ching ESC, Guo H, Lo TS. 2008b. Refined similarity hypotheses in shell models of homogeneous turbulence and turbulent convection. *Phys. Rev. E* 78:026303
Ching ESC, Guo H, Shang XD, Tong P, Xia KQ. 2004b. Extraction of plumes in turbulent thermal convection. *Phys. Rev. Lett.* 93:124501
Ching ESC, Ko TC. 2008. Ultimate-state scaling in a shell model for homogeneous turbulent convection. *Phys. Rev. E* 78:036309

Ching ESC, Kwok CY. 2000. Statistics of local temperature dissipation in high Rayleigh number convection. *Phys. Rev. E* 62:R7587–90
Ching ESC, Leung CK, Qiu XL, Tong P. 2003b. Intermittency of velocity fluctuations in turbulent thermal convection. *Phys. Rev. E* 68:026307
Cioni S, Ciliberto S, Sommeria J. 1995. Temperature structure functions in turbulent convection at low Prandtl number. *Europhys. Lett.* 32:413–18
Corrsin S. 1951. On the spectrum of isotropic temperature fluctuations in anisotropic turbulence. *J. Appl. Phys.* 22:469–73
Effinger H, Grossmann S. 1987. Static structure function of turbulent flow from the Navier-Stokes equation. *Z. Phys. B* 66:289–304
Eggers J, Grossmann S. 1991. Does deterministic chaos imply intermittency in fully-developed turbulence? *Phys. Fluids A* 3:1958–68
Emran MS, Schumacher J. 2008. Fine-scale statistics of temperature and its derivatives in convective turbulence. *J. Fluid Mech.* 611:13–34
Falkovich G, Gawędzki K, Vergassola M. 2001. Particles and fields in fluid turbulence. *Rev. Mod. Phys.* 73:913–75
Frisch U. 1995. *Turbulence*. Cambridge, UK: Cambridge Univ. Press
Funfschilling D, Brown E, Ahlers G. 2008. Torsional oscillations of the large-scale circulation in turbulent Rayleigh-Bénard convection. *J. Fluid Mech.* 607:119–39
Gasteuil Y, Shew WL, Gibert M, Chillá F, Castaing B, Pinton JF. 2007. Lagrangian temperature, velocity, and local heat flux measurement in Rayleigh-Bénard convection. *Phys. Rev. Lett.* 99:234302
Glazier JA, Segawa T, Naert A, Sano M. 1999. Evidence against ultrahard thermal turbulence at very high Rayleigh numbers. *Nature* 398:307–10
Gluckman BJ, Willaime H, Gollub J. 1993. Geometry of isothermal and isoconcentration surfaces in thermal turbulence. *Phys. Fluids A* 5:647–61
Grossmann S, Lohse D. 1991. Fourier-Weierstrass mode analysis for thermally driven turbulence. *Phys. Rev. Lett.* 67:445–48
Grossmann S, Lohse D. 1992a. Intermittency in Navier-Stokes dynamics. *Z. Phys. B* 89:11–19
Grossmann S, Lohse D. 1992b. Scaling in hard turbulent Rayleigh-Bénard flow. *Phys. Rev. A* 46:903–17
Grossmann S, Lohse D. 1993. Characteristic scales in Rayleigh-Bénard convection. *Phys. Lett. A* 173:58–62
Grossmann S, Lohse D. 2000. Scaling in thermal convection: a unifying view. *J. Fluid. Mech.* 407:27–56
Grossmann S, Lohse D. 2001. Thermal convection for large Prandtl number. *Phys. Rev. Lett.* 86:3316–19
Grossmann S, Lohse D. 2002. Prandtl and Rayleigh number dependence of the Reynolds number in turbulent thermal convection. *Phys. Rev. E* 66:016305
Grossmann S, Lohse D. 2004. Fluctuations in turbulent Rayleigh-Bénard convection: the role of plumes. *Phys. Fluids* 16:4462–72
Grossmann S, Lohse D, L'vov V, Procaccia I. 1994. Finite size corrections to scaling in high Reynolds number turbulence. *Phys. Rev. Lett.* 73:432–35
Grossmann S, L'vov VS. 1993. Crossover of spectral scaling in thermal turbulence. *Phys. Rev. E* 47:4161–68
Hartmann DL, Moy LA, Fu Q. 2001. Tropical convection and the energy balance at the top of the atmosphere. *J. Clim.* 14:4495–511
He X, Tong P. 2009. Measurements of the thermal dissipation field in turbulent Rayleigh-Bénard convection. *Phys. Rev. E* 79:026306
He X, Tong P, Xia KQ. 2007. Measured thermal dissipation field in turbulent Rayleigh-Bénard convection. *Phys. Rev. Lett.* 98:144501
Heslot F, Castaing B, Libchaber A. 1987. Transition to turbulence in helium gas. *Phys. Rev. A* 36:5870–73
Ishihara T, Gotoh T, Kaneda Y. 2009. Study of high-Reynolds number isotropic turbulence by direct numerical simulation. *Annu. Rev. Fluid Mech.* 41:165–80
Julien K, Legg S, McWilliams J, Werne J. 1999. Plumes in rotating convection. Part 1. Ensemble statistics and dynamical balances. *J. Fluid Mech.* 391:151–87
Kaczorowski M, Wagner C. 2009. Analysis of the thermal plumes in turbulent Rayleigh-Bénard convection based on well-resolved numerical simulations. *J. Fluid Mech.* 618:89–112

Kadanoff LP. 2001. Turbulent heat flow: structures and scaling. *Phys. Today* 54(8):34–39
Kerr R. 1996. Rayleigh number scaling in numerical convection. *J. Fluid Mech.* 310:139–79
Kerr RM. 2001. Energy budget in Rayleigh-Bénard convection. *Phys. Rev. Lett.* 87:244502
Kolmogorov AN. 1941. The local structure of turbulence in imcompressible viscous fluid for very large Reynolds numbers. *Dokl. Akad. Nauk. SSSR* 30:299–303
Krishnamurti R, Howard LN. 1981. Large scale flow generation in turbulent convection. *Proc. Natl. Acad. Sci. USA* 78:1981–85
Kunnen RPJ, Clercx HJH, Geurts BJ, Bokhoven LJA, Akkermans RAD, Verzicco R. 2008. A numerical and experimental investigation of structure function scaling in turbulent Rayleigh-Bénard convection. *Phys. Rev. E* 77:016302
Kurien S, Sreenivasan KR. 2000. Anisotropic scaling contributions to high-order structure functions in high-Reynolds-number turbulence. *Phys. Rev. E* 62:2206–12
Kuznetsov EA, L'vov VS. 1981. On developed hydrodynamic turbulence spectra. *Phys. D* 2:203–17
Landau LD, Lifshitz EM. 1987. *Fluid Mechanics*. Oxford: Pergamon
Lohse D. 1994. Temperature spectra in shear flow and thermal convection. *Phys. Lett. A* 196:70–75
Lohse D, Müller-Groeling A. 1996. Anisotropy and scaling corrections in turbulence. *Phys. Rev. E* 54:395–405
Lohse D, Toschi F. 2003. The ultimate state of thermal convection. *Phys. Rev. Lett.* 90:034502
Lukaschuk S, Ashkenazi S, Lebedev V, Steinberg V. 2001. New light scattering technique based on phase time derivative correlation function. *Europhys. Lett.* 56(6):808–14
Lumley JL. 1967. Similarity and turbulent energy spectrum. *Phys. Fluids* 10:855–58
Marshall J, Schott F. 1999. Open-ocean convection: observations, theory, and models. *Rev. Geophys.* 37:1–64
Mashiko T, Tsuji Y, Mizuno T, Sano M. 2004. Instantaneous measurement of velocity fields in developed thermal turbulence in mercury. *Phys. Rev. E* 69:036306
McKenzie DP, Roberts JM, Weiss NO. 1974. Convection in the Earth's mantle: towards a numerical simulation. *J. Fluid Mech.* 62:465–538
Moisy F, Willaime H, Andersen J, Tabeling P. 2001. Passive scalar intermittency in low temperature helium flows. *Phys. Rev. Lett.* 86:4827–30
Monin AS, Yaglom AM. 1975. *Statistical Fluid Mechanics*. Cambridge, MA: MIT Press
Niemela J, Skrbek L, Sreenivasan KR, Donnelly R. 2000. Turbulent convection at very high Rayleigh numbers. *Nature* 404:837–40
Niemela J, Sreenivasan KR. 2006. The use of cryogenic helium for classical turbulence: promises and hurdles. *J. Low Temp. Phys.* 143:163–212
Nikolaenko A, Brown E, Funfschilling D, Ahlers G. 2005. Heat transport by turbulent Rayleigh-Bénard convection in cylindrical cells with aspect ratio one and less. *J. Fluid Mech.* 523:251–60
Obukhov AM. 1949. Structure of the temperature field in a turbulent flow. *Izv. Akad. Nauk. SSSR Ser. Geog. Geofiz.* 13:58–69
Obukhov AM. 1959. On the influence of Archimedean forces on the structure of the temperature field in a turbulent flow. *Dokl. Akad. Nauk. SSR* 125:1246–48
Pinton JF, Labbé R. 1994. Correction to the Taylor hypothesis in swirling flows. *J. Phys. II France* 4:1461–68
Pope SB. 2000. *Turbulent Flow*. Cambridge, UK: Cambridge Univ. Press
Procaccia I, Ching ESC, Constantin P, Kadanoff LP, Libchaber A, Wu XZ. 1991. Transition to convective turbulence: the role of thermal plumes. *Phys. Rev. A* 44:8091–102
Procaccia I, Zeitak R. 1989. Scaling nonisotropic convective turbulence. *Phys. Rev. Lett.* 62:2128–31
Procaccia I, Zeitak R. 1990. Scaling exponents in thermally driven turbulence. *Phys. Rev. A* 42:821–30
Puthenveettil BA, Arakeri JH. 2005. Plume structure in high-Rayleigh-number convection. *J. Fluid Mech.* 542:217–49
Qiu XL, Yao SH, Tong P. 2000. Large-scale coherent rotation and oscillation in turbulent thermal convection. *Phys. Rev. E* 61:R6075–78
Rahmstorf S. 2000. The thermohaline ocean circulation: a system with dangerous thresholds? *Clim. Change* 46:247–56
Richardson LF. 1926. Atmospheric diffusion shown on a distance-neighbor graph. *Proc. R. Soc. Lond. Ser. A* 110:709–37

Rincon F. 2006. Anisotropy, inhomogeneity and inertial-range scalings in turbulent convection. *J. Fluid Mech.* 563:43–69
Rubio MA, Bigazzi P, Albavetti L, Ciliberto S. 1989. Spatio-temporal regimes in Rayleigh-Bénard convection in a small rectangular cell. *J. Fluid Mech.* 209:309–34
Ruiz-Chavarria G, Baudet C, Ciliberto S. 1996. Scaling laws and dissipation scale of a passive scalar in fully developed turbulence. *Phys. D* 99:369–80
Saddoughi SG, Veeravalli SV. 1994. Local isotropy in turbulent boundary layers at high Reynolds number. *J. Fluid Mech.* 268:333–72
Sano M, Wu XZ, Libchaber A. 1989. Turbulence in helium-gas free-convection. *Phys. Rev. A* 40:6421–30
Schumacher J. 2008. Lagrangian dispersion and heat transport in convective turbulence. *Phys. Rev. Lett.* 100:134502
Shang XD, Xia KQ. 2001. Scaling of the velocity power spectra in turbulent thermal convection. *Phys. Rev. E* 64:065301
Shang XD, Qiu XL, Tong P, Xia KQ. 2003. Measured local heat transport in turbulent Rayleigh-Bénard convection. *Phys. Rev. Lett.* 90:074501
She ZS, Jackson E. 1993. On the universal form of energy spectra in fully developed turbulence. *Phys. Fluids A* 5:1526–28
She ZS, Lévêque E. 1994. Universal scaling laws in fully developed turbulence. *Phys. Rev. Lett.* 72:336–39
Shishkina O, Wagner C. 2006. Analysis of thermal dissipation rates in turbulent Rayleigh-Bénard convection. *J. Fluid Mech.* 546:51–60
Shishkina O, Wagner C. 2008. Analysis of sheetlike thermal plumes in turbulent Rayleigh-Bénard convection. *J. Fluid Mech.* 599:383–404
Shraiman BI, Siggia ED. 1990. Heat transport in high-Rayleigh number convection. *Phys. Rev. A* 42:3650–53
Siggia ED. 1994. High Rayleigh number convection. *Annu. Rev. Fluid Mech.* 26:137–68
Skrbek L, Niemela JJ, Sreenivasan KR, Donnelly RJ. 2002. Temperature structure functions in the Bolgiano regime of thermal convection. *Phys. Rev. E* 66:036303
Sreenivasan KR. 1991. On local isotropy of passive scalars in turbulent shear flows. *Proc. R. Soc. Lond. A* 434:165–82
Sreenivasan KR, Antonia RA. 1977. Skewness of temperature derivatives in turbulent shear flows. *Phys. Fluids* 20:1986–88
Sreenivasan KR, Antonia RA. 1997. The phenomenology of small-scale turbulence. *Annu. Rev. Fluid Mech.* 29:435–72
Sun C, Cheung YH, Xia KQ. 2008. Experimental studies of the viscous boundary layer properties in turbulent Rayleigh-Bénard convection. *J. Fluid Mech.* 605:79–113
Sun C, Xia KQ. 2007. Multi-point local temperature measurements inside the conducting plates in turbulent thermal convection. *J. Fluid Mech.* 570:479–89
Sun C, Xia KQ, Tong P. 2005. Three-dimensional flow structures and dynamics of turbulent thermal convection in a cylindrical cell. *Phys. Rev. E* 72:026302
Sun C, Zhou Q, Xia KQ. 2006. Cascades of velocity and temperature fluctuations in buoyancy-driven thermal turbulence. *Phys. Rev. Lett.* 97:144504
Takeshita T, Segawa T, Glazier JA, Sano M. 1996. Thermal turbulence in mercury. *Phys. Rev. Lett.* 76:1465–68
Taylor GI. 1938. The spectrum of turbulence. *Proc. R. Soc. Lond. A* 164:476–90
Tennekes H, Lumley JL. 1972. *A First Course in Turbulence*. Cambridge, MA: MIT Press
Tong P, Shen Y. 1992. Relative velocity fluctuations in turbulent Rayleigh-Bénard convection. *Phys. Rev. Lett.* 69:2066–69
Toschi F, Amati G, Succi S, Benzi R, Piva R. 1999. Intermittency and structure functions in channel flow turbulence. *Phys. Rev. Lett.* 82:5044–47
Vainshtein S, Sreenivasan K. 1994. Kolmogorov's 4/5 law and intermittency in turbulence. *Phys. Rev. Lett.* 73:3085–88
Verzicco R, Camussi R. 2003. Numerical experiments on strongly turbulent thermal convection in a slender cylindrical cell. *J. Fluid Mech.* 477:19–49
von der Heydt A, Grossman S, Lohse D. 2001. Scaling exponents in anisotropic turbulence from the Navier-Stokes equations. *J. Fluid Mech.* 440:381–90

Warhaft Z. 2000. Passive scalars in turbulent flows. *Annu. Rev. Fluid Mech.* 32:203–40
Wittmer KS, Devenport WJ, Zsoldos JS. 1998. A four-sensor hot-wire probe system for three-component velocity measurement. *Exp. Fluids* 24:416–23
Wu XZ, Kadanoff L, Libchaber A, Sano M. 1990. Frequency power spectrum of temperature-fluctuation in free convection. *Phys. Rev. Lett.* 64:2140–43
Xi HD, Lam S, Xia KQ. 2004. From laminar plumes to organized flows: the onset of large-scale circulation in turbulent thermal convection. *J. Fluid Mech.* 503:47–56
Xia KQ, Sun C, Zhou SQ. 2003. Particle image velocimetry measurement of the velocity field in turbulent thermal convection. *Phys. Rev. E* 68:066303
Yakhot V. 1992. 4/5 Kolmogorov law for statistically staionary turbulence: application to high Rayleigh number Bénard convection. *Phys. Rev. Lett.* 69:769–71
Zhang J, Wu XL. 2005. Velocity intermittency in a buoyancy subrange in a two-dimensional soap film convection experiment. *Phys. Rev. Lett.* 94:234501
Zhang J, Wu XL, Xia KQ. 2005. Density fluctuations in strongly stratified two-dimensional turbulence. *Phys. Rev. Lett.* 94:174503
Zhou Q, Sun C, Xia KQ. 2007. Morphological evolution of thermal plumes in turbulent Rayleigh-Bénard convection. *Phys. Rev. Lett.* 98:074501
Zhou Q, Sun C, Xia KQ. 2008. Experimental investigation of homogeneity, isotropy, and circulation of the velocity field in buoyancy-driven turbulence. *J. Fluid Mech.* 598:361–72
Zhou Q, Xia KQ. 2008. Comparative experimental study of local mixing of active and passive scalars in turbulent thermal convection. *Phys. Rev. E* 77:056312
Zhou SQ, Xia KQ. 2001. Scaling properties of the temperature field in convective turbulence. *Phys. Rev. Lett.* 87:064501
Zhou SQ, Xia KQ. 2002. Plume statistics in thermal turbulence: mixing of an active scalar. *Phys. Rev. Lett.* 89:184502

Annual Review of
Fluid Mechanics

Volume 42, 2010

Contents

Indexes

Errata

An online log of corrections to *Annual Review of Fluid Mechanics* articles may be found at http://fluid.annualreviews.org/errata.shtml